



# Global Biogeochemical Cycles<sup>a</sup>

#### RESEARCH ARTICLE

10.1029/2023GB007991

#### **Key Points:**

- Implemented a trait-based model of dynamic phytoplankton elemental stoichiometry within global biogeochemical simulations
- Dynamic stoichiometry decreased phytoplankton P-limitation in the tropics and subtropics and increased Nfixation and export
- Frugal P-utilization in low P environments and increased P-rich ribosomes at high growth rates leave distinct biogeochemical fingerprints

#### **Supporting Information:**

Supporting Information may be found in the online version of this article.

#### Correspondence to:

G. I. Hagstrom, georgehagstrom@gmail.com

#### Citation:

Hagstrom, G. I., Stock, C. A., Luo, J. Y., & Levin, S. A. (2024). Impact of dynamic phytoplankton stoichiometry on global scale patterns of nutrient limitation, nitrogen fixation, and carbon export. *Global Biogeochemical Cycles*, 38, e2023GB007991. https://doi.org/10.1029/2023GB007991

Received 5 OCT 2023 Accepted 20 APR 2024

#### **Author Contributions:**

Conceptualization: George I. Hagstrom, Charles A. Stock, Jessica Y. Luo, Simon A. Levin

**Formal analysis:** Charles A. Stock, Jessica Y. Luo

Funding acquisition: George I. Hagstrom, Charles A. Stock, Jessica Y. Luo, Simon A. Levin

**Methodology:** George I. Hagstrom, Charles A. Stock, Jessica Y. Luo, Simon A. Levin

**Software:** George I. Hagstrom, Charles A. Stock, Jessica Y. Luo **Validation:** George I. Hagstrom

© 2024. The Authors.

This is an open access article under the terms of the Creative Commons

Attribution License, which permits use, distribution and reproduction in any medium, provided the original work is properly cited.

# Impact of Dynamic Phytoplankton Stoichiometry on Global Scale Patterns of Nutrient Limitation, Nitrogen Fixation, and Carbon Export

George I. Hagstrom<sup>1</sup>, Charles A. Stock<sup>2</sup>, Jessica Y. Luo<sup>2</sup>, and Simon A. Levin<sup>1</sup>

<sup>1</sup>Department of Ecology and Evolutionary Biology, Princeton University, Princeton, NJ, USA, <sup>2</sup>NOAA Geophysical Fluid Dynamics Laboratory, Princeton, NJ, USA

**Abstract** Phytoplankton stoichiometry modulates the interaction between carbon, nitrogen and phosphorus cycles. Environmentally driven variations in phytoplankton C:N:P can alter biogeochemical cycling compared to expectations under fixed ratios. In fact, the assumption of fixed C:N:P has been linked to Earth System Model (ESM) biases and potential misrepresentation of responses to future change. Here we integrate key elements of the Adaptive Trait Optimization Model (ATOM) for phytoplankton stoichiometry with the Carbon, Ocean Biogeochemistry and Lower Trophics (COBALT) ocean biogeochemical model. Within a series of global ocean-ice-ecosystem retrospective simulations, ATOM-COBALT reproduced observations of phytoplankton N:P, and compared to static ratios, exhibited reduced phytoplankton Plimitation, enhanced N-fixation, and increased low-latitude export, improving consistency with observations and highlighting the biogeochemical implications of dynamic N:P. We applied ATOM-COBALT to explore the impacts of different physiological mechanisms hypothesized to underlie N:P variation, finding that two mechanisms together drove the observed patterns: proportionality of P-rich ribosomes in phytoplankton cells to growth rates and reductions in P-storage during scarcity. A third mechanism which linked temperature with phytoplankton biomass allocations to non-ribosomal proteins, led only to relatively modest impacts because this mechanism decreased the temperature dependence of phytoplankton growth rates, compensating for changes in N:P. We find that there are quantitative response differences that associate distinctive biogeochemical footprints with each mechanism, which are most apparent in highly productive low-latitude regions. These results suggest that variable phytoplankton N:P makes phytoplankton productivity and export resilient to environmental changes, and support further research on the physiological and environmental drivers of phytoplankton stoichiometry and biogeochemical role.

Plain Language Summary Marine phytoplankton are single-celled photosynthetic organisms that live near the ocean's surface, where they absorb carbon dioxide and other nutrients. This exerts a large influence on ocean chemistry and, through the ocean's capacity to absorb carbon dioxide from the atmosphere, the Earth's climate. We explored how phytoplankton vary their requirements for two essential nutrients, nitrogen and phosphorus, based on environmental conditions, and how that variation affects the export of carbon from the surface ocean to depth. We found that flexibility in phytoplankton nutrient uptake ratios makes them use phosphorus more efficiently, driving an increase in carbon export. It also stimulates nitrogen fixation, causing an increase in nitrogen available to phytoplankton. As a result, our simulations predicted significantly less phosphorus limitation and more export from low-latitude parts of the ocean, increasing agreement with observations. Flexible phytoplankton nutrient requirements change how marine ecosystems respond to the environment, and understanding how these nutrient requirements vary is key to predicting how the ocean will respond to future changes.

# 1. Introduction

Marine phytoplankton facilitate carbon (C) sequestration from the atmosphere to the deep ocean, forming a crucial part of the biological carbon pump and regulating ocean chemistry and global climate. Primary productivity and C-export tightly couple to the biogeochemical cycles of nitrogen (N), phosphorus (P), and iron (Fe), because the availability of these resources can limit the growth of phytoplankton. The elemental stoichiometry of phytoplankton, defined as the ratio of C:N:P in the organic matter of their cells, helps determine how strongly the C, N, and P cycles interact.

HAGSTROM ET AL. 1 of 23



# **Global Biogeochemical Cycles**

10.1029/2023GB007991

Writing – original draft: George I. Hagstrom, Charles A. Stock, Jessica Y. Luo, Simon A. Levin Writing – review & editing: George I. Hagstrom, Charles A. Stock, Jessica Y. Luo, Simon A. Levin A prominent and useful paradigm in biological oceanography holds that C:N:P ratios can be approximated as constants that reflect global means, known as the *Redfield Ratios* (Redfield, 1958) (typically 106:16:1). However, recent observations reveal systematic variations of the C:N:P of organic matter, exceeding Redfield in subtropical gyres and the tropics and falling below Redfield in high-latitudes (Martiny, Pham, et al., 2013). This has consequences for the C-cycle and the response of the oceans to global change, impacting relationships between nutrient availability and export, as well as feedbacks that depend on physiological mechanisms that regulate C:N:P (Deutsch & Weber, 2012; Galbraith & Martiny, 2015; Moreno et al., 2018).

Despite recent observations of variations in phytoplankton elemental stoichiometry, Earth System Models (ESMs) rarely capture dynamic C:N:P, with most opting to use Redfield ratios or fixed stoichiometry for different phytoplankton size classes (Danabasoglu et al., 2020; Séférian et al., 2020). While these models capture many large-scale observed biogeochemical patterns, static stoichiometry has been linked to a number of significant biases. For example, the relatively comprehensive Carbon Ocean Biogeochemistry and Lower Trophics (CO-BALT) ocean biogeochemical model used in Earth System simulations contributed by the Geophysical Fluid Dynamics Laboratory to the 6th Coupled Model Intercomparison Project (CMIP6) (J. Dunne et al., 2020; Stock et al., 2020) imposed static characteristic C:N:P ratios for each of three phytoplankton types. This led to muted N: P variations and was linked to an over-expression of P-limitation and a suppression of nitrogen fixation (Stock et al., 2020). Similar issues arose in other ESMs using fixed or highly simplified C:N:P ratios (Martiny et al., 2019), leading to a growing number of efforts to address this limitation in ESMs (Kwiatkowski et al., 2018; Long et al., 2021; Tanioka & Matsumoto, 2017).

Several mechanisms have been proposed to explain the observed C:N:P patterns (Moreno & Martiny, 2018). The *growth rate hypothesis* holds that rapidly growing cells require more P-rich ribosomes (Elser et al., 2000), leading to lower C:N:P in eutrophic ecosystems and higher in oligotrophic ones. The *translation compensation hypothesis* suggests that the increased efficiency of protein synthesis in warmer waters relative to photosynthesis (Devault, 1980) leads to fewer ribosomes and higher C:N:P in warm waters. Lastly, the *frugality hypothesis* postulates that cells decrease their quota of scarce resources, causing C:N:P to anti-correlate with phosphate (Galbraith & Martiny, 2015) due to higher plasticity of P-quotas compared with C and N. Covariation between observed temperature, nutrients, and food web structure had previously hindered attempts to disentangle these mechanisms, discouraging the use of dynamic C:N:P in biogeochemical models.

Observational advances, however, have facilitated recent papers (Bopp et al., 2022; Chien et al., 2023; Kwiatkowski et al., 2018; Kwon et al., 2022; Matsumoto et al., 2020; Moreno et al., 2018; Pahlow et al., 2020), which study the centrality of these mechanisms for the current and future controls on carbon export and nitrogen fixation, through both direct changes in nutrient utilization and novel interactions driven by differences in C:N:P between ocean regions and lateral nutrient transport.

Future ocean warming may cause an expansion of oligotrophic gyres, with projected negative impacts on primary productivity, carbon export, and biomass available for higher trophic levels (Bopp et al., 2013; Moore et al., 2018). However, high phytoplankton diversity could enable phytoplankton to rapidly adapt to warmer, lower nutrient conditions, possibly mitigating these expected changes (G. I. Hagstrom & Levin, 2017; Martiny, Hagstrom, et al., 2022). Dynamic phytoplankton N:P provides one mechanism whereby plankton can buffer against these environmental shifts, however in order to study the potential for this to occur, biogeochemical models need to better capture the adaptive capacity of phytoplankton.

To answer these questions, we integrated elements of ATOM (Adaptive Trait Optimization Model), a *trait-based model* (Litchman & Klausmeier, 2008) of phytoplankton C:N:P (C. A. Garcia et al., 2020; Moreno et al., 2018), with the Carbon, Ocean, Biogeochemistry, and Lower Trophics (COBALT) marine ecosystem model (Stock et al., 2014, 2020). We ask the following questions: (a) how do phytoplankton stoichiometric ratios and nutrient limitation patterns in the global oceans emerge from ecosystem dynamics, (b) how do these stoichiometric ratios impact marine ecosystem function and biogeochemical cycling of carbon, nitrogen, phosphorus and iron, (c) what role do each of the following three mechanisms (growth rate, translation compensation, and frugality) play in determining biogeochemical patterns?

HAGSTROM ET AL. 2 of 23

19449224, 2024, 5, Downloaded from https://agupubs.onlinelibrary.wiley.com/doi/10.1029/2023GB007991 by Princeton University, Wiley Online Library on [23.07/2024]. See the Terms and Conditions (https://onlinelibrary.wiley.com/doi/10.1029/2023GB007991 by Princeton University, Wiley Online Library on [23.07/2024]. See the Terms and Conditions (https://agupubs.onlinelibrary.wiley.com/doi/10.1029/2023GB007991 by Princeton University, Wiley Online Library on [23.07/2024]. See the Terms and Conditions (https://agupubs.onlinelibrary.wiley.com/doi/10.1029/2023GB007991 by Princeton University, Wiley Online Library on [23.07/2024]. See the Terms and Conditions (https://agupubs.onlinelibrary.wiley.com/doi/10.1029/2023GB007991 by Princeton University, Wiley Online Library on [23.07/2024]. See the Terms and Conditions (https://agupubs.onlinelibrary.wiley.com/doi/10.1029/2023GB007991 by Princeton University, Wiley Online Library on [23.07/2024]. See the Terms and Conditions (https://agupubs.onlinelibrary.wiley.com/doi/10.1029/2023GB007991 by Princeton University, Wiley Online Library on [23.07/2024]. See the Terms and Conditions (https://agupubs.onlinelibrary.wiley.com/doi/10.1029/2023GB007991 by Princeton University (https://agupubs.com/doi/10.1029/2023GB007991 by Princ

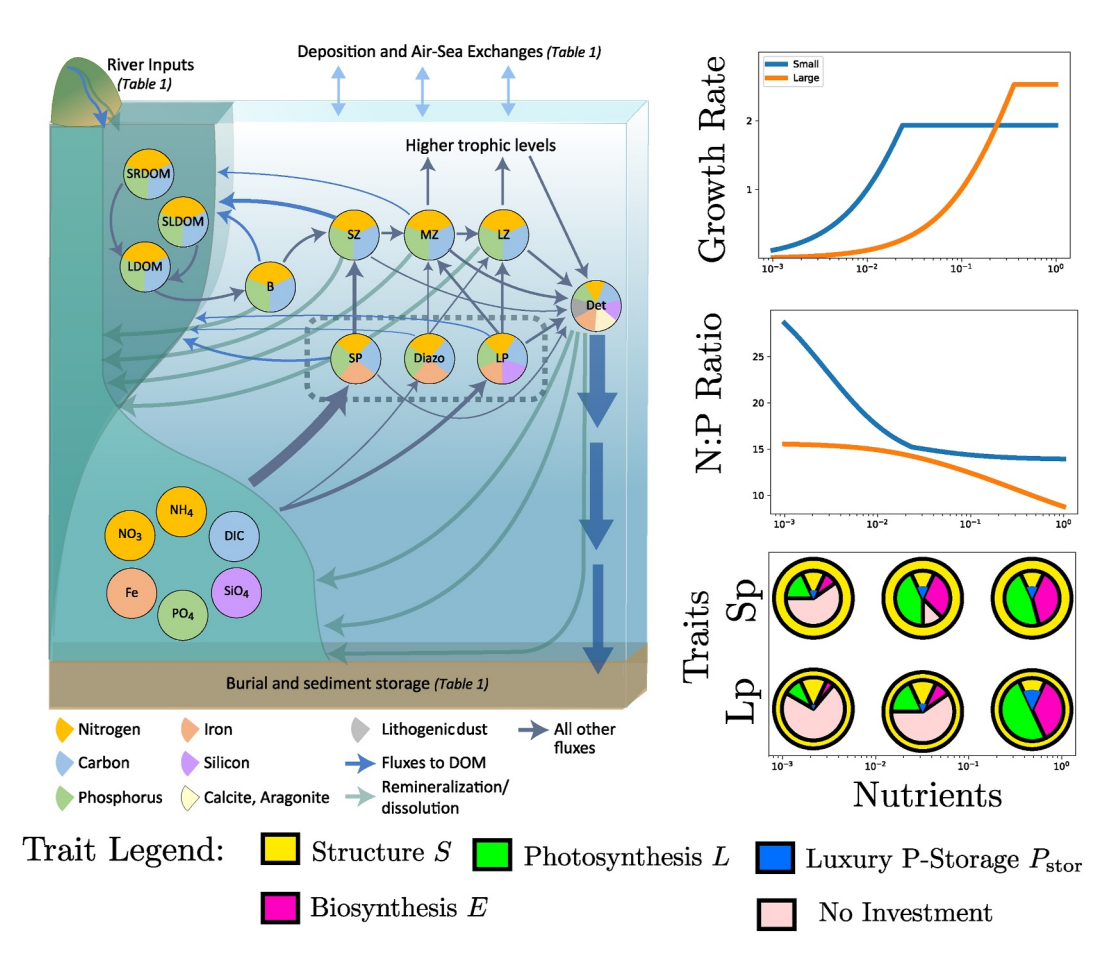


**Figure 1.** COBALT food web model and modifications to incorporate dynamic stoichiometry and ATOM. The diagram on the left hand-side of the figure shows the COBALT food web model (Stock et al., 2020), illustrating the different tracer pools and the fluxes between them due to food web interactions and biogeochemical dynamics. The pie-charts in the COBALT figure qualitatively indicate the different elements that comprise each pool. A rectangle marks the three phytoplankton pools, which are modeled differently in ATOM-COBALT. The modifications to the large, small, and diazotrophic phytoplankton are described in the far right hand side column, which shows the functional response of large and small phytoplankton to nutrient concentrations (with the x-axis indicating increasing nitrate, ammonium, and phosphate), the response of N:P ratios, and the optimal trait values for low, medium, and high levels of nutrients. The optimal trait-values are shown quantitatively using pie-charts, not to be confused with the pie-charts from the original COBALT figure. No investment corresponds to solutions that involve cells investing less than their full volume in biosynthesis, photosynthesis, and structure.

#### 2. Methods

#### 2.1. COBALT

The base configuration of COBALT simulates global scale cycles of carbon, nitrogen, phosphorus, iron, silica, calcite, aragonite, and lithogenic materials using 33 tracers, 3 distinct phytoplankton pools, 3 zooplankton pools, and a single bacterial pool (Stock et al., 2014, 2020). The most pertinent aspect for integration with ATOM is the formulation for phytoplankton growth and nutrient uptake, which we describe here. COBALT represents three size classes of phytoplankton, a small phytoplankton parameterized to emulate cyanobacteria like *Synechococcus* and *Prochlorococcus*, a large phytoplankton parameterized to emulate diatoms, and a diazotroph parameterized to emulate *Trichodesmium* (see Figure 1, upper left). We will denote the differences between phytoplankton types by the subscripts (*sp*, *lp*, *diazo*) for small, large, and diazotroph, in expressions where the types have different functional responses. Following Geider (Geider et al., 1997), COBALT modeled the growth rate of a phytoplankton population using the following expression:

HAGSTROM ET AL. 3 of 23

$$\mu = \frac{P_{cm}}{1+\zeta} \left( 1 - \exp\left(\frac{-\alpha_{Pl}\theta Irr}{P_{cm}}\right) \right) \tag{1}$$

where  $P_{cm}$  is the maximum photosynthesis rate allowed by a given temperature and nutrient concentration,  $\zeta$  is the cost of biosynthesis,  $\alpha_{PI}$  is the Chl-specific initial slope of the photosynthesis-irradiance curve,  $\theta$  is the Chl-carbon ratio, and Irr is the instantaneous irradiance.

The Chl:carbon ratio depends on the past history of irradiance Irr<sub>mem</sub>:

$$\theta = \frac{(\theta_{\text{max}} - \theta_{\text{min}})}{\left(1 + \frac{\theta_{\text{max}} \alpha_{P} \text{Ir}_{\text{mem}}}{2P_{cm}}\right)} + \theta_{\text{min}}.$$
 (2)

The  $Irr_{mem}$  is calculated based on the past history of irradiance (averaged over the actively mixed layer), updated at each time step to provide an estimate of the mean daytime irradiance, which is used to calculate the Chl:carbon ratio. To facilitate the estimation of daytime irradiance, phytoplankton at each grid point also store an estimate of the day length.

In COBALT we assume that  $P_{cm}$  depends on nutrient limitation and temperature according to:

$$P_{cm} = P_{c\text{max}} \exp(\kappa_{\text{eppley}} T) \text{ nutlim}, \tag{3}$$

where  $\kappa_{\text{eppley}}$  is the temperature scaling factor following Eppley (1972), T is measured in degrees Celsius, and nutlim is a number between 0 and 1 that depends on nutrient concentrations and the internal iron quota via Liebig's law of the minimum.

Inorganic nitrogen or phosphorus concentrations, or the internal iron quota, can limit the growth of the small or large phytoplankton, with modeled competition between nitrate and ammonium uptake following O'Neill et al. (1989). COBALT chooses a formulation based on Liebig's Law of the Minimum (von Liebig, 1840), whereby phytoplankton growth rates depend only on the concentration of the most limiting of several different nutrients:

$$\operatorname{nutlim}_{sp,lp} = \min((N)_{\lim_{sp,lp}}, (PO_4)_{\lim_{sp,lp}}, (Fe)_{\lim_{sp,lp}}),$$
(4)

where (suppressing the subscript for now):

$$(PO_4)_{lim} = \frac{[PO_4]}{K_{PO_4} + [PO_4]}$$
 (5)

$$(\text{Fe})_{\text{lim}} = \frac{(Q_{\text{Fe:N}})^2}{(Q_{\text{Fe:N}})^2 + (K_{Q_{\text{Fe:N}}})^2}$$
(6)

$$(N)_{lim} = (NO_3)_{lim} + (NH_4)_{lim}$$
 (7)

$$(NO_3)_{lim} = \frac{[NO_3]}{[NO_3] + K_{NO_3} + [NH_4] \frac{K_{NO_3}}{K_{NH_4}}}$$
(8)

$$(NH_4)_{lim} = \frac{[NH_4]}{[NH_4] + K_{NH_4} + [NO_3] \frac{K_{NH_4}}{K_{NO_3}}}$$
(9)

Diazotrophs fix nitrogen and thus their growth does not depend on nitrogen limitation:

$$\operatorname{nutlim}_{diazo} = \min((PO_4)_{\lim_{diazo}}, (Fe)_{\lim_{diazo}}), \tag{10}$$

HAGSTROM ET AL. 4 of 23

however, COBALT allows diazotrophs to take up nitrate and ammonium if at sufficiently high concentrations, reducing the contribution of nitrogen fixation to their growth. COBALT defines  $(N)_{lim,di}$  using the same mathematical expression as for other phytoplankton types, and uses it to determine the rate of nitrate and ammonium uptake:

$$J_{\text{up,NH}_4,diazo} = \mu_{diazo}(\text{NH}_4)_{\text{lim }diazo} \tag{11}$$

$$J_{\text{up,NO}_3,diazo} = \mu_{diazo}(\text{NO}_3)_{\text{lim,diazo}}.$$
(12)

Biomass in the three zooplankton pools represented in COBALT has a fixed N:P ratio different from that of the phytoplankton types. The COBALT food web model determines the ingestion rates of prey by each zooplankton type in a given grid cell, which allows calculation of the total ingestion rate of organic N and P for each zooplankton type. A fraction of initially ingested organic matter is immediately lost to the detritus and dissolved organic matter pools in a manner that maintains stoichiometric ratios. The remaining flux of organic matter, which is available for growth and respiration, is here called  $J_{\text{net},N,(smz,mdz,lgz)}$  and  $J_{\text{net},P,(smz,mdz,lgz)}$  to represent the net flux of N and P available for growth to each zooplankton pool. Zooplankton excrete excess N and P above their growth needs as [NH<sub>4</sub>] and [PO<sub>4</sub>], according to the formula:

$$J_{\text{ex,N,}(smz,mdz,lgz)} = J_{\text{prod,N,}(smz,mdz,lgz)} - J_{\text{net,N,}(smz,mdz,lgz)}$$
(13)

$$J_{\text{ex},N,(smz,mdz,lgz)} = J_{\text{prod},N,(smz,mdz,lgz)}(N:P)_{(smz,mdz,lgz)} - J_{\text{net},P,(smz,mdz,lgz)}$$
(14)

Here the  $J_{\rm ex}$  terms describe the excretion of inorganic N and P. Zooplankton production is a function of ingested N and P, and is determined by a minimum of the flux of P relative to stoichiometric requirements and the flux of C relative to respiration, growth efficiency, and growth requirements. Because of the fixed C:N ratio of organic matter, zooplankton cannot be N limited.

#### **2.2. ATOM**

ATOM (C. A. Garcia et al., 2020; Moreno et al., 2018) is a *trait-based* (Litchman & Klausmeier, 2008) phytoplankton model that uses the principle of optimal resource allocation (Shuter, 1979; Smith et al., 2011) to calculate phytoplankton traits- including cell radius, biomass allocations to photosynthesis, biosynthesis, structure, and luxury phosphorus storage (Figure 1, right side and bottom). These trait values determine modeled phytoplankton cells' functional response to environmental conditions and C:N:P ratio. ATOM models phytoplankton growth rates as limited by the slowest of several different physiological processes: carbon acquisition, nitrogen acquisition, phosphorus acquisition, and biosynthesis (the synthesis of proteins and other biological macromolecules present in the cell). Carbon acquisition depends on the level of light and the biomass allocation to photosynthesis according to the model published in Talmy et al. (2013), with the exact adaptation to ATOM published in Moreno et al. (2018) and (C. A. Garcia et al., 2020). Nutrient affinity depends linearly on cell radius according to laws governing diffusion limited uptake (Purcell, 1977), which determines uptake rates of phosphate and nitrate/ammonium. Luxury phosphorus storage increases hyperbolically as a function of environmental concentrations of phosphate. Together, these investments and the level of luxury storage determine the macromolecular (proteins, lipids, RNA, carbohydrates, etc) composition of the phytoplankton cell and therefore its elemental stoichiometry through the ratios of each type of macromolecule.

ATOM calculates the trait values by assuming that all phytoplankton cells have trait values that optimize their growth rate (Shuter, 1979). This (unique) growth optimum occurs at the trait values which make specific biosynthetic, photosynthetic, and either nitrogen or phosphorus uptake rates equal. ATOM incorporates the growth rate hypothesis, translation compensation hypothesis, and frugality through the physiological mechanisms that give rise to these hypotheses (e.g., optimal radius, investment in P-rich biosynthetic apparatus varies across oligotrophic-eutrophic spectrum, different temperature dependence of physiological processes leads to translation compensation, and luxury storage captures frugality).

HAGSTROM ET AL. 5 of 23

#### 2.3. Integration of ATOM Stoichiometry With COBALT

The ATOM-COBALT dynamic stoichiometry model (also referred to herein as simply the "dynamic model") introduced here adds the subcellular resource compartments used in ATOM to each phytoplankton type in COBALT. Compared to COBALT-v2 (Stock et al., 2020), ATOM-COBALT also adds an additional tracer to each phytoplankton group, the phytoplankton phosphorus content. ATOM-COBALT models four trait values for each phytoplankton type, calculating each dynamically from environmental conditions every time step and using the result to predict the N:P uptake of each phytoplankton type. Here we model only dynamics of the N:P ratio due to its greater plasticity compared with C:N (Galbraith & Martiny, 2015) and due to the existence of physiological mechanisms which explain its variability (Moreno & Martiny, 2018). The traits are allocations of biomass to biosynthesis (E), carbon fixation ( $F_1$ ), electron transport and light harvesting ( $F_2$ ), and luxury phosphorus storage  $P_{stor}$ . Together, the carbon fixation and electron transport compartments form the photosynthesis compartment, defined by  $L = F_1 + F_2$ , and throughout most of the paper we will refer only to L and not  $F_1$  or  $F_2$ , as the relative ratio between the two will be shown to be a function of irradiance.

The units of investments in E and L are specific biomass (Nitrogen per unit Nitrogen). The values thus represent a fraction of the overall biomass dedicated to each purpose. We constrain the maximum total investment in E and L, which decreases with cell radius (therefore different for small, large, and diazotroph) because the cell membrane and associated structures are typically of fixed thickness and thus have a biomass proportional to the surface area, rather than the volume, of the cell (Shuter, 1979; Toseland et al., 2013):

$$S_{sp,lp,diazo} + E + L \le 1, \quad E \ge 0, \quad L \ge 0,$$
 (15)

where S is the structural investment, and we allow for cells with  $E + L + S \le 1$ . Here  $S_{sp,lp,diazo}$  are constant values characterizing each phytoplankton type, while E and L are dynamical variables updated in each grid cell at each time-step. Allowing this sum to be less than 1 (which corresponds to the areas of no-investment shown in Figure 1) enables the fixed size classes to exhibit similar responses to those in the original ATOM model where the radius trait is part of the optimization. This model feature approximates several different aspects of phytoplankton physiology and ecology, including the fixed size classes representing organisms with a range of different cell radii or cells increasing their surface area to volume ratio.

We derive the phytoplankton functional response as a function of the traits, and assume that phytoplankton make investments in traits that optimize their growth rate (Shuter, 1979). Because each compartment has a different elemental composition, the investment in traits will determine the relative uptake of nitrogen and phosphorus, and therefore the elemental stoichiometry of each phytoplankton type. This allows the trait-based model to encode the physiological and ecological mechanisms determining phytoplankton N:P ratios.

To derive the functional response in terms of traits, we assume that cells with a given set of traits  $(E, F_1, F_2)$  grow at the minimum rate implied by three biochemical processes: nutrient acquisition, macromolecule synthesis, and carbon acquisition.

$$\mu = \min(\mu_{\text{nut}}, \mu_{\text{synth}}, \mu_{\text{light}}) \tag{16}$$

We assume that

$$\mu_{\text{nut}} = P_{c\text{max}} \text{nutlim}, \tag{17}$$

where we calculate nutlim using the same functional response in COBALT: a Michaelis-Menten function for nitrogen and phosphorus limitation (using (O'neill et al., 1989) to capture ammonium and nitrate limitation and uptake) and a functional form based on the internal iron quota for iron limitation (Equation 9).

Synthesis limitation depends on the investment in biosynthesis:

$$\mu_{\text{synth}} = P_{c\text{max}} E, \tag{18}$$

and light limitation on the investments in carbon fixation  $(F_1)$  and electron transport  $(F_2)$ :

HAGSTROM ET AL. 6 of 23

$$\mu_{\text{light}} = \frac{P_{\text{m}} \left( 1 - \exp\left(-\frac{\alpha \phi_{\text{M}} F_{2} \text{Irr}}{P_{\text{m}}}\right) \right) - bresp}{1 + \zeta}.$$
 (19)

Here,  $P_{\rm m}$ , the maximum light-limited photosynthesis rate, depends on the investments in  $F_1$  and  $F_2$  (see Table 1 for parameter definitions and values):

$$P_{\rm m} = \min(k_1 \, F_1, \, k_2 \, F_2). \tag{20}$$

The investment in electron transport proteins  $F_2$  is analogous to the Chl:C ratio that determines the growth rates in COBALT and in the original Geider formulation (Talmy et al., 2013), allowing Chl:C to be calculated from  $F_2$  through multiplication by 0.075 and normalization by the total cellular investment S + E + L.

For given environmental conditions, we model phytoplankton allocations by assuming they adopt trait values E and L that lead to growth rate maximization. In our model, there are two possible scenarios for optimal solutions. In the first scenario the implied growth rates from nutrient limitation, biosynthesis, and photosynthesis and photosynthesis balance so that cell growth is co-limited by all three of these processes:  $\mu_{\text{nut}} = \mu_{\text{light}} = \mu_{\text{synth}}$ . This solution, which we call ( $E_{\text{co}}$ ,  $L_{\text{co}}$ ), is a valid solution if it satisfies the constraint  $S + E_{\text{co}} + L_{\text{co}} \le 1$ , which says that the total biomass investment into structure, biosynthesis, and photosynthesis must be less than or equal to 1. If the co-limited solution is valid, we set the actual allocations equal to the co-limited solution  $E = E_{\text{co}}$  and  $E = E_{\text{co}}$ . The total investment is less than 1 in this scenario, meaning that part of the cell volume has no investment (this corresponds to the first two columns in the traits plot in the lower right hand corner of Figure 1). The possibility for a cell to have investment less than 1 is a consequence of combining the trait structure of ATOM (which varies cell radius to find the optimal traits) and the fixed size structure of COBALT, and we interpret  $E = E_{\text{co}}$  and  $E = E_{\text{co}}$  and the fixed size structure of COBALT, and we interpret  $E = E_{\text{co}}$  and  $E = E_{\text{co}}$  and the fixed size structure of COBALT, and we interpret  $E = E_{\text{co}}$  and  $E = E_{\text{co}}$  and the fixed size structure of COBALT, and we interpret  $E = E_{\text{co}}$  and  $E = E_{\text{co}}$  and  $E = E_{\text{co}}$  and the fixed size structure of COBALT, and we interpret  $E = E_{\text{co}}$  and  $E = E_{\text{co}}$  are the first value  $E = E_{\text{co}}$  and  $E = E_{\text{co}}$  are the first value  $E = E_{\text{co}}$  and E =

If the co-limited solution is not valid then nutrient concentrations are so high that it is not possible to balance nutrient limitation with biosynthesis and photosynthesis. In this scenario we find a solution which balances photosynthesis and biosynthesis and fully invests all the volume of the cell:  $\mu_{light} = \mu_{synth}$  and S + E + L = 1. We call the solution to this set of equations ( $E_{rep}$ ,  $L_{rep}$ ). This solution corresponds to growth rate maximization in an environment where nutrients are replete. If the co-limited solution is invalid, we set the actual allocations equal to the nutrient replete solution  $E = E_{rep}$  and  $E = E_{rep}$ . This can be seen in the third column of the traits plot in the bottom left of Figure 1.

We show the full details of this solution procedure in Text S2 of the Supporting Information S1. It involves solving a nonlinear equation for the balance between carbon fixation and electron transport proteins ( $F_1$  and  $F_2$ ) at fixed total photosynthesis investment L, which leads to a linear equation for the balance between the overall photosynthesis investment L and the biosynthesis investment E. We use an offline routine to solve the non-linear equation and approximate it using a Fourier-Chebyshev series, enabling us to efficiently calculate optimal solutions. To accommodate the diel cycle of irradiance, we adopt an irradiance memory formulation similar to that of COBALT where the cell determines the optimal investment in L based on the history of past irradiance (averaged over the actively mixed layer) and an estimate of the length of the light period, where the optimization assumes constant irradiance during the light period.

To calculate phytoplankton N:P we specify the specific N and P content of each subcellular compartment and add a luxury P-storage compartment to the model. We denote the nitrogen and phosphorus contents of each compartment with parameters (see Table 1).  $N_S$  and  $P_S$  represent the N and P content of the structure pool in g/g dryWeight.  $N_{prot}$  is the average N-content of proteins, which is equal to the N-content of the photosynthesis pool because that pool is modeled as containing only proteins. The biosynthesis pool contains a mixture of proteins and RNA, but the N-content of RNA is nearly equal to that of proteins so that one constant  $(N_{prot})$  is sufficient to describe the N-content of both pools. The photosynthesis pool does not contain any P.  $P_E$  represents the P content of the biosynthetic pool, and  $P_{stor}$  is the content of the storage pool with units of g/gDryWeight (and hence a dynamic model variable rather than a parameter). Using these terms, we can calculate the stoichiometry of a cell

HAGSTROM ET AL. 7 of 23

	Source	
	Definition	
	Units	
r Definitions, and Values	Value	
<b>Table 1</b> List of Model Parameters, Their	Parameter and variables	
·		

Parameter and variables	Value	Units	Definition	Source
$\mathrm{E}_{((sp,lp,diazo))}$	Dynamic	None	Biosynthesis Investment	Modeled
$\mathbf{L}_{((sp,lp,diazo))}$	Dynamic	None	Photosynthesis Investment	Modeled
$\mathbf{P}_{ ext{stor},(sp,lp,diazo)}$	Dynamic	gP/gDry	P-content of Storage pool	Modeled
Keppley	0.063	1/(deg Celsius)	T-dependence of biosynthetic machinery	Eppley (1972)
Kphoto	0-0.063	1/(deg Celsius)	T-dependence of photosynthetic machinery	Devault (1980) and Raven and Geider (1988)
$P_{cmax,((sp,lp,diazo))}$	(1.25, 1.25, 0.5)	1/day	Biosynthetic efficiency at 0 Celsius	Capone et al. (1997) and Geider et al. (1997)
$\zeta_{(sp,lp,diazo)}$	(0.25, 0.25, 0.75)	None	Carbon cost of synthesis	Tuned Shuter (1979)
bresp <sub>(sp,lp,diazo)</sub>	(0.03, 0.05, 0.05)	1/day	Specific respiration rate at 0 Celsius	Tuned Stock et al. (2014)
$k_{1,0}$	0.145	1/day	Efficiency of carbon fixation machinery 0 Celsius	Talmy et al. (2013)
$k_{2,0}$	0.333	1/day	Efficiency of electron transport chain proteins 0 Celsius	Talmy et al. (2013)
$lpha_{ph,(sp,lp,diazo)}$	(1.972, 0.6573, 0.6573)	$gC/m^2$	Carbon specific initial slope of PI curve	Talmy et al. (2013)
LFac	1.2	None	Light harvesting investment adjusted factor	Tuned
$\Phi_M$	1.0e6	gC/µmol photons	Quantum Efficiency	Talmy et al. (2013)
$\mathbf{P}_{StorMax((sp,lp,diazo))}$	(0.01, 0.025, 0.01)	gP/gDry	Maximum luxury phosphorus storage	Tuned
$S_{ m struc,((sp,lp,diazo))}$	(0.4625, 0.2, 0.4625)	None	Structure Investment	Tuned Shuter (1979) and Toseland et al. (2013)
$K_{{ m NO}_3,((arphi,lp,diazo))}$	(2.5e - 7, 2.5e - 7, 2.5e - 6)	mmolNO <sub>3</sub> /m <sup>3</sup>	Half saturation constant for nitrate	Stock et al. (2014)
$K_{\mathrm{NH_4},((sp,lp,diazo))}$	(5e - 8, 1e - 7, 5e - 7)	$\mathrm{mmolNH_4/m}^3$	Half saturation constant for ammonium	Stock et al. (2014)
$K_{\mathrm{PO_4},((sp,lp,diazo))}$	(1e - 8, 1e - 7, 1e - 7)	$\text{mmolPO}_4/\text{m}^3$	Half saturation constant for phosphate	Stock et al. (2014)
$K_{PStor,((sp,lp,diazo))}$	(2.5e - 8, 1e - 6, 1e - 6)	$\text{mmolPO}_4/\text{m}^3$	Half saturation constant for luxury storage	Tuned
$K_{Q}$ Fe,(( $sp,lp,diazo$ ))	(1.98e - 5, 3.97e - 5, 1.656e - 4)	mol Fe/mol N	Half saturation constant for internal iron quota	Stock et al. (2014)
$N_{S,(sp,lp,diazo)}$	0.128	gN/gDry	N-content of Structure pool	Tuned based on Sterner and Elser (2017)
$N_{\mathrm{prot},(sp,lp,diazo)}$	0.16	gN/gDry	N-content of protein	Sterner and Elser (2017)
$\mathbf{P}_{\mathbf{S},(sp,lp,diazo)}$	(3.5e - 3, 5e - 3, 2e - 3)	gP/gDry	P-content of Structure pool	Tuned based on Sterner and Elser (2017)
${ m P}_{{ m E},(sp,lp,diazo)}$	5e - 2	gP/gDry	P-content of Biosynthesis pool	Tuned based on Sterner and Elser (2017) and Toseland et al. (2013)

Note. Dynamically calculated trait values appear in the initial rows.

using the strategy (E, L) and with luxury storage  $P_{stor}$ , by summing the N and P contents of each compartment and taking the quotient of the result:

$$N:P = \frac{(SN_S + (E+L)N_{prot}) Mol_P}{(EP_E + SP_S + P_{stor}) Mol_N}$$
(21)

Here  $\mathrm{Mol_N}$  and  $\mathrm{Mol_P}$  are the mass in grams of 1 mol of nitrogen and phosphorus, respectively. The values of the N and P content parameters and the allocation to the structural pool S can be derived from cell radius and the macromolecular composition of each pool, though these compositions are also uncertain. Here we treat the N and P content parameters of each subcellular compartment as fundamental, tunable parameters in the model, however, we constrained the choice for these parameters using our knowledge of their macromolecular composition (which is quantified more explicitly in several papers (Daines et al., 2014; C. A. Garcia et al., 2020; Shuter, 1979; Sterner & Elser, 2017)). Relative to the Redfield ratio, the biosynthesis pool is rich in P and the structural and photosynthesis pool are poor in P.

The structure pool S consists of a fraction corresponding to the cell wall; membrane; and periplasmic space, and also static components of the cytoplasm (such as DNA, RNA, lipids, carbohydrates, and housekeeping proteins). The cell wall and membrane space have a fixed thickness, and thus the value of S is inversely proportional to cell radius, so that  $S_{sm} = S_{di} > S_{1g}$ . The N content of the structure pool is modeled as the same for each type, but  $P_{S,di} < P_{S,sm} < P_{S,lg}$  to capture the capacity for small phytoplankton to utilize sulfolipids instead of phospholipids in their cell membranes, and the tendency for diazotrophs to be highly efficient at P-utilization, enabling them to reach higher N:P ratios than other phytoplankton. Phospholipids in small phytoplankton and diazotrophs are modeled as luxury storage of P.

Luxury P storage has slightly different parameterizations in large phytoplankton than in diazotrophs and small phytoplankton. In both cases luxury storage increases hyperbolically as a function of phosphate concentrations, but for large phytoplankton the overall level of storage is scaled by the total investment so that it is proportional to cytoplasmic volume:

$$P_{stor,lp} = \frac{P_{stor,max}[P]}{K_{P,stor} + [P]} (S_{lp} + E_{lp} + L_{lp})$$
(22)

Here [P] refers to the ambient concentration of phosphate in the environment.

For small phytoplankton and diazotrophs, luxury P-storage is parameterized to reflect the P-content in phospholipid membranes, which can be substituted for sulfoquinovosyl diacylglycerol (SQDG) at low phosphorus concentrations (Van Mooy et al., 2006). SQDG contains sulfur instead of phosphorus and SQDG substitution reduces phytoplankton P-quotas. We therefore scale the luxury storage term to be proportional to the size of the structure pool, which is the pool in the cell that contains lipid membranes:

$$P_{stor,sp,di} = \frac{P_{stor,max}[P]}{K_{P,stor} + [P]} S_{sp,di}$$

The half-saturation constants for luxury storage,  $K_{P,stor}$ , are greater than the corresponding half-saturation constant for phosphorus limitation of each type, and the parameter  $P_{stor,max}$ , which is the maximum possible level of P-storage, varies between the small and large phytoplankton and diazotrophs (see Table 1). In small phytoplankton and diazotrophs, these constants correspond to a storage pool represented by membrane phospholipids and therefore are smaller than the constant in large phytoplankton, which are known to store much greater quantities of phosphorus and reach much lower N:P ratios in P-rich conditions (Rhee, 1974). The scaling to the level of total investment moderates the level of luxury storage in environments where iron or nitrogen is highly limiting.

The N-content of the biosynthesis and photosynthesis pool are assumed to be the same as that of proteins, reflecting the fact that these pools are primarily proteins and RNA which have nearly identical N-content. The P-content of biosynthesis pool depends on the ratio of ribosomes to proteins in the biosynthetic apparatus, which is a free parameter that controls how strongly N:P ratios change with growth rate. The parameter choice represents an

HAGSTROM ET AL. 9 of 23

approximate 50% split between ribosomes and other proteins in the biosynthesis apparatus, consistent with other parameterizations (Toseland et al., 2013) and with fits of the ATOM model to data (C. A. Garcia et al., 2020). Figure 3; Text S2 and Figure S1 in Supporting Information S1 show how the optimal strategies vary globally in numerical simulations, and how these shifts lead the emergence of model N:P ratios.

The optimal strategy determines the N:P ratio of nutrient uptake, which causes the N:P ratio of phytoplankton to approach that of the optimal strategy:

$$J_{\text{NO}_3} = \mu \frac{\text{NO}_{3\text{lim}}}{(\text{NO}_3)_{\text{lim}} + (\text{NH}_4)_{\text{lim}}}$$
(23)

$$J_{\text{NH}_4} = \mu \frac{(\text{NH}_4)_{\text{lim}}}{(\text{NO}_3)_{\text{lim}} + (\text{NH}_4)_{\text{lim}}}$$
(24)

$$J_{PO_4} = \frac{J_{NO_3} + J_{NH_4}}{(N:P)} \tag{25}$$

The  $P_{cmax}$  and bresp parameters depend on temperature exponentially through the constant  $\kappa_{eppley}$ , but a new temperature dependence is introduced through  $\kappa_{photo}$ , allowing for exploration of the translation compensation hypothesis:

$$k_1 = k_{1,0} \exp(\kappa_{\text{photo}} T), \quad k_2 = k_{2,0} \exp(\kappa_{\text{photo}} T)$$
 (26)

Here  $k_{1,0}$  and  $k_{2,0}$  refer to the specific efficiency of the carbon fixation and light harvesting proteins at 0 degrees Celsius (Table 1). Irradiance has a substantial impact on the temperature dependence of growth rates because  $\kappa_{\text{photo}}$  cancels from the right hand side of Equation 19 for small *Irr*. We illustrate the impact of both irradiance and  $\kappa_{\text{photo}}$  on modeled growth rates and allocations in Text S3 of the Supporting Information S1.

### 2.4. Alternative Models

Considerable uncertainty still exists about the relative contribution of the growth rate hypothesis, translation compensation, and frugality to phytoplankton elemental stoichiometry. In order to explore the potential impacts of each of these mechanisms on biogeochemical cycles, we developed a series of alternative models each emphasizing one of the physiological mechanisms, as well as a static control model used to understand the magnitude of the effects of using dynamic stoichiometry.

#### 2.4.1. Static Control Model

We developed a static control model which uses the functional response of the ATOM-COBALT dynamic model but maintains the static ratios used by COBALT:

$$(N:P)_{sm} = 22$$
,  $(N:P)_{lg} = 12$ ,  $(N:P)_{diazo} = 40$ 

This ensures that the differences between the static control and the fully dynamic ATOM-COBALT model arise because of dynamic stoichiometry rather than differences in other aspects of the functional response, such as growth rates. Because the functional response has changed from the standard COBALT implementation (Stock et al., 2020), simulations using the static control model may differ from those using standard COBALT.

#### 2.4.2. Frugal Model

The second alternative is the *frugal model*, again using the same functional response as the ATOM-COBALT model but modeling N:P based on the concentration of phosphate, following (Galbraith & Martiny, 2015):

(N:P) = 
$$\frac{1}{3.1 \times 10^{-2} + 4.818 \times 10^{4} [PO_4]}$$

HAGSTROM ET AL. 10 of 23

In this model small and large phytoplankton and diazotrophs have the same N:P. Figure 1 illustrates this mechanism through the increase in stored P with phosphate.

#### 2.4.3. Growth Rate Model

The third alternative model is called the *growth rate model* and focuses on the growth rate hypothesis, excluding frugality by setting to a constant the level of luxury-P storage in each of the small, large, and diazotroph types. We modified the models by setting the stored-P equal to a fraction of the maximum in each type:

$$P_{\text{stor}} = 0.3P_{\text{stor,max}}$$

Thus the N:P of each type only varies according to the growth rate. In Figure 1, this mechanism corresponds to the increase in biosynthetic allocation with increased nutrients and light.

#### 2.4.4. Dynamic Plus Translation Compensation Model

The final alternative is called the *dynamic plus translation compensation model* (or Dynamic plus Trans. Comp.). Translation compensation occurs when the temperature dependence of photosynthetic and biosynthetic processes differ. In the fully dynamic model we assume these dependencies are the same, but in the translation compensation model we make photosynthetic proteins and pigments temperature independent by setting the exponential constant equal to 0:

$$\kappa_{\rm photo} = 0.0$$

We also shift the value of the parameters  $k_{1,0}$  and  $k_{2,0}$  so that they have the same values as they would in the dynamic model at T = 15 Celsius, which maintains roughly the same average value of  $k_1$  and  $k_2$  across the two simulations. After this shift, we have:

$$k_{1,0} = 0.37332, k_{2,0} = 0.8568$$

This changes both the optimal balance between photosynthetic and biosynthetic investments (E and L) and the overall functional response of growth rates to temperature. In the translation compensation model, growth rates will be lower in warm waters and higher in cold waters compared to the fully dynamic model, assuming identical environmental conditions. However, due to the form of Equation 19 for the photosynthetic functional response, the impact of temperature on growth rates becomes irradiance dependent, so that even in the dynamic model there is a translation compensation effect under low irradiance conditions. Text S3 in Supporting Information S1 explores these issues in more detail.

#### 2.4.5. Observational Data

We gathered data sets from 36 different cruises and long-term time series sites that contained measurements of the N:P of particulate organic matter in the surface ocean (Table S1 in Supporting Information S1). To avoid biases induced by highly variable sampling frequencies between different cruises, we binned samples from the top 100 m sampled on the same day. Selected cruises provide coverage of most ocean regions and biomes, and the majority of data comes from recent, intensive GO-SHIP expeditions (Tanioka, Larkin, et al., 2022).

# 2.4.6. Numerical Experiments

We embedded the static control model, the dynamic model, and each alternative model within a series of oceanice-ecosystem retrospective simulations using the GFDL Modular Ocean Model 6 (MOM6) and Sea Ice Simulator 2 (SIS2), using a nominal  $0.5^{\circ}$  horizontal grid spacing (OM4p5 (Adcroft et al., 2019)). The vertical grid uses 75 vertical layers in hybrid  $z^{\star}$ -isopycnal coordinates implemented through an Arbitrary Lagrangian-Eulerian method that applies the  $z^{\star}$  coordinate near the surface and the isopycnal coordinates in the ocean interior. The ocean and ice model configurations match those within the fully coupled ESM4.1 model (J. Dunne et al., 2020). Model simulations were forced using the Common Ocean-Ice Reference Experiment II (Large & Yeager, 2009), a 60-year data set representing atmospheric forcings from 1948 to 2007. Initial conditions were chosen similar to

HAGSTROM ET AL. 11 of 23

the fully coupled model (Stock et al., 2020): from World Ocean Atlas 2013 (WOA13) data for temperature, salinity, oxygen, and dissolved inorganic nutrients (H. E. Garcia et al., 2013; H. Garcia et al., 2014), and from the Global Ocean Data Analysis Project (GLODAPv2) for dissolved inorganic carbon and alkalinity (Lauvset et al., 2016). Initial conditions for other tracers were derived from outputs of a previous version of COBALT (Stock et al., 2014), and initial conditions for additional tracers corresponding to small, large, and diazotroph phosphorus were derived based on assumed constant ratios in each pool. We specify external nutrient fluxes including atmospheric NH<sub>4</sub> and NO<sub>3</sub> deposition (Horowitz et al., 2003), Fe deposition from dust (Zhao et al., 2018) using Baker and Croot to calculate Fe solubility. Coastal Fe and river nutrients derive from the GlobalNEWS data set (Seitzinger et al., 2005), following the prescription in Stock et al. (2020). Five model simulations captured 60 years of ocean dynamics, the reported results come from climatology computed from the last 20 years of each simulation.

#### 2.4.7. Biogeographic Analysis

We defined ocean biomes for biogeographic analyses by dividing the surface grid points from numerical simulations into four bins based on latitude and chlorophyll concentrations. The biomes correspond to the subpolar ocean (above 45N/S), mid-latitude (between 23.5N/S and 45N/S) high chlorophyll, tropical (between 23.5S and 23.5N) high chlorophyll, and oligotrophic (below 45N/S and low chlorophyll), and are calculated separately for each simulation. For observational data, we set the boundary between high and low chlorophyll to a surface concentration of 0.125 mg/m³, following the definition in Polovina et al. (2011). Due to variations in the food web structure in the static and dynamic models, we selected distinct chlorophyll thresholds for each model so that the total area of high and low chlorophyll areas matches the biome definitions in Polovina et al. (2011).

We classify nutrient limitation by comparing the Liebig factors (see Equation 9) for N, P, and Fe limitation in small phytoplankton (and P and Fe for diazotrophs), weighted by productivity to de-emphasize winter periods in polar regions where nutrient limitation isn't meaningful. Strong limitation implies that one of the nutrients is substantially more limiting than the other two (a difference of Liebig factors of more than 0.2), and weak limitation means either that two or more nutrients are very close to equally limiting, or that the Liebig factor is quite close to 1.

# 3. Results

#### 3.1. Overall Model Results and Latitudinal Patterns of N:P

The ATOM-COBALT simulation with dynamic stoichiometry produced a mean global N:P value of 21 (spatial average of N:P of export), with a middle 66th percentile range of 16.8–26.4, consistent with observations (Martiny et al., 2014; Tanioka, Larkin, et al., 2022), see Table 2 and Figure 2. N:P ratios exhibited a strong spatial pattern, with low ratios in high-export regions and high ratios in low-export regions, so that the ratio of total N-Export to total P-Export was 16.4 in the dynamic stoichiometry simulations, consistent with the Redfield ratio (Figure 5). Global NPP and total export out of the top 100 m were also within range, at 53.0 and 8.2 PgC/yr, respectively, consistent with observational constraints (Behrenfeld et al., 2005; J. P. Dunne et al., 2007; Kulk et al., 2020).

ATOM-COBALT simulations with dynamic stoichiometry produce N:P ratios with more variability than the static control (Figures 2 and 4a), exhibiting greater consistency with observed stoichiometric variations across ocean biomes. Simulations with dynamic stoichiometry produced geometric mean N:P ratios that were on average over 30% higher than static controls in the subtropical gyres (25.0 vs. 18.9, observations are 24.4) and 20% higher in the high-chlorophyll tropics (20.7 vs. 17.4, observations are 20.4), and 21% higher in the mid-latitude high-chlorophyll regions (19.5 vs. 16.1, observations are 19.0), with nearly equal values in the high-latitudes (13.8 vs. 14.2, observations 14.2). Outside of the subpolar oceans, where both models had similar mean N:P, the dynamic model was closer to observational data. The dynamic model produced a much larger range of values than the static model, both within and across biomes, though neither model had as variable a distribution as the observations.

The strong latitudinal gradients in N:P ratios in the dynamic model reflect the global patterns of traits (Figure 3), which show increasing investments in E, L, and S + E + L moving from the center of oligotrophic gyres outwards toward more eutrophic areas (Figure 3). In low nutrient ecosystems, the structure pool dominates the P-quota,

HAGSTROM ET AL. 12 of 23

 Table 2

 Global Net Primary Productivity, Carbon Export, and N:P of Exported Organic Matter (Geometric Mean of Annually Averaged N:P at Each Grid-Cell)

Measure	Static control	Dynamic	Obs.
NPP PgC/yr	46.9	53.0	38.8-52.1 (Behrenfeld et al., 2005; Kulk et al., 2020)
Export PgC/yr	7.5	8.2	5.8–12.9 (J. P. Dunne et al., 2007)
Export N:P	17.3 (15.0, 19.5)	21.0 (16.8, 26.1)	20.9 (13.9, 31.4) (Martiny et al., 2014) (Tanioka, Larkin et al., 2022)
Plankton Nut. Lim.	(0.41N, 0.23 Fe, 0.36 P)	(0.68N, 0.24 Fe, 0.08 P)	
Diazotroph Nut. Lim.	(0.37 Fe, 0.63 P)	(0.49 Fe, 0.51 P)	

with greater contributions from biosynthesis and storage in eutrophic and high latitude regions. Both the growth rate hypothesis and the frugality hypothesis thus drive the observed N:P ratios in the dynamic model.

#### 3.2. Biogeographic Comparison Between Dynamic and Static Simulations

Considering patterns of nutrient limitation, the introduction of dynamic N:P stoichiometry substantially reduced large areas of phosphorus limitation that arose in the static-control (see Figures 4b and 4c, and the ESM4.1 simulation with similar settings (Stock et al., 2020)). In the dynamic simulations, N-limitation occurs throughout the North and South Pacific subtropical gyres and the eastern half of the tropics, in the entire Indian Ocean, and most of the Atlantic Ocean, with the exception of the boundary between the North Atlantic subtropical gyre and the high-latitude North Atlantic, which is weakly P-limited. Fe-limitation occurs in the traditional High-Nutrient Low-Chlorophyll (HNLC) regions. On the other hand, static simulations show large areas of P-limitation, particularly near anthropogenic N-inputs or other regions where nutrient supply is enriched with N relative to P, such as the entire North Atlantic subtropical gyre and transition zones between the Indian and South Pacific subtropical gyres and the Southern Ocean. Overall, there is a 79% decrease in the areal extent of P-limitation from 36% in the static control to 8% in the dynamic ATOM simulation. Here we plotted nutrient limitation of small phytoplankton. Large phytoplankton had similar nutrient limitation patterns but exhibited more weak limitation by a secondary nutrient, a difference caused by low concentrations of both N and P well below the large phytoplankton saturation constants in oligotrophic regions.

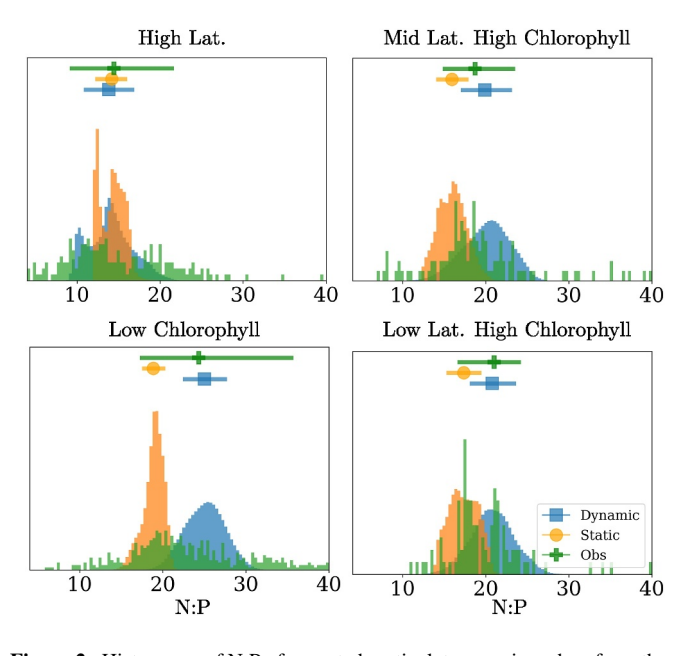


**Figure 2.** Histograms of N:P of exported particulate organic carbon from the ATOM-COBALT dynamic model, static control model, and observational data at grid points binned by latitude and chlorophyll, with bins chosen to sort grid points and observational data according to ocean biome.

A smaller decrease of P-limited areas occurred for diazotrophs, by 20% from 75% in the static controls to 61% in the dynamic simulations, where we restricted the calculation of areas to latitudes lower than 40° where most N-fixation occurs. In the static simulations, very little Fe-limitation occurs in the subtropical gyres, in contrast to the dynamic simulations where parts of the North and South Pacific subtropical gyres have Fe-limited diazotrophs. The greater range of N:P ratios in the fully dynamic simulations increases the N:P supply threshold at which phytoplankton switch from N to P limitation.

The reduction in P-limited areas evident in Figures 4b and 4c is accompanied by an enhancement in nitrogen fixation (Figure 4d) in the dynamic simulations. Nitrogen fixation can occur in ecosystems where the phytoplankton in the surface primarily experience N-limitation. N-limitation usually implies that P and Fe are sufficiently replete to support a niche for diazotrophs. A portion of the fixed nitrogen is recycled and makes further contributions to the productivity of the ecosystem. This surface source allows the N:P ratio of export to exceed the N:P ratio in the nutrient supply from deep waters. Consistent with the observation that the fully dynamic model had reductions in areas of P-limitation, overall nitrogen fixation in this simulation was approximately 100% higher than in the static controls, 171 Tg N/yr compared with 90 Tg N/yr. This increase brings predictions more closely in line with observations (Table 3). We observed this broadly across low-latitude regions, including the tropical and subtropical Atlantic, the Indian Ocean, and the Western Pacific. In total, the overall increase in N-fixation in subtropical gyres was 170% and in tropical and low-latitude coastal ecosystems was 70%.

HAGSTROM ET AL. 13 of 23

19449224, 2024, 5, Downloaded from https://agupubs.onlinelibrary.wiley.com/doi/10.1029/2023GB007991 by Princeton University, Wiley Online Library on [23/07/2024]. See the Terms and

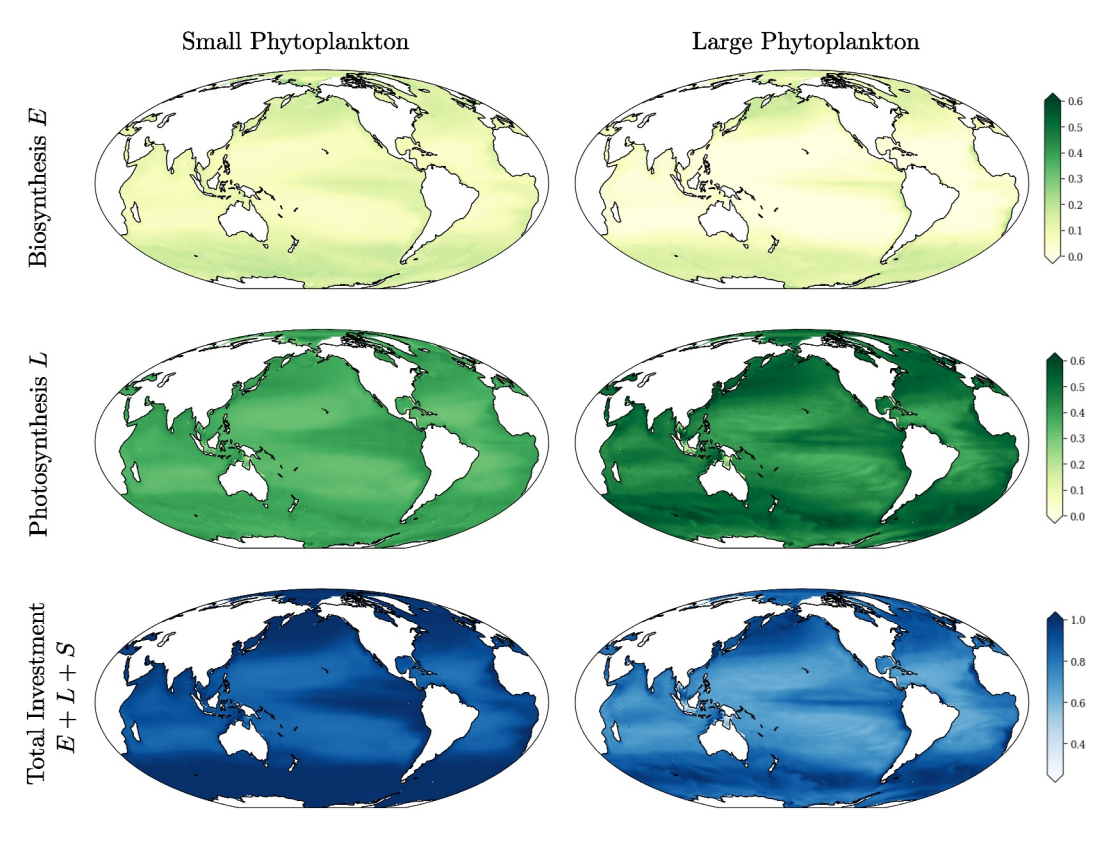


**Figure 3.** Biomass and productivity weighted average of biosynthesis, photosynthesis, and total investment trait values in small and large phytoplankton.

A decrease in N-fixation compared with the static simulations occurred in the HNLC Eastern Equatorial Pacific (see also Figure 7a).

Dynamic stoichiometry caused an increase in export of 0.7 PgC/yr, driven primarily by the relaxation of P-limitation of diazotrophs and phytoplankton in the subtropics and tropics (Figure 4e). The change in export roughly parallels the changes in both N:P ratios and nitrogen fixation, suggesting that a shift to higher N:P and the resulting increase in nitrogen availability from diazotrophs explains increases in export. Overall, export increased by 10% in the dynamic simulations compared to control, driven by a 14% increase in the tropical and low-latitude coastal ecosystems and a 30% increase in subtropical gyres, bringing estimates from ATOM-COBALT more in line with observations (Emerson, 2014). The increase in export was accompanied by a modest expansion of

**Table 3**Observationally Derived Estimates of Global N-Fixation Compared to Model Simulations

Source	Global N-fixation (Tg N/yr)
Luo et al. (2012)	137
Großkopf et al. (2012)	177
Tang et al. (2019)	197.1
Wang et al. (2019)	163.2
Dynamic Model (this work)	184
Static Model (this work)	92
Dynamic w. Trans. Comp. (this work)	194
Growth Rate (this work)	171
Frugal Model (this work)	233

oxygen minimum zones and denitrification (30%), which partially offsets the increase N-fixation under dynamic N:P. The simulations performed here are not long enough to observe the equilibration of the deep ocean N-cycle.

# 3.3. Biogeochemical Fingerprints of Stoichiometry Drivers

Comparison between the dynamic simulation and the alternative stoichiometry model simulations revealed the biogeochemical imprint of each modeled physiological mechanism influencing N:P ratios (Figures 5–8). Three fundamental patterns emerged: (a) frugality decreases P-limitation more strongly than the growth rate mechanism, driving comparatively higher N-fixation and export; (b) the growth rate mechanism produces stronger gradients in N:P between eutrophic coastal and tropical regions and oligotrophic subtropical regions, which has a large impact on nitrogen fixation patterns; and (c) the dynamic model with translation compensation causes little change in the N:P ratio and other large scale biogeochemical patterns compared to the dynamic model.

HAGSTROM ET AL. 14 of 23

19449224, 2024, 5, Downloaded from https://agupubs.onlinelibrary.wiley.com/doi/10.1029/2023GB007991 by Princeton University, Wiley Online Library on [23:07/2024]. See the Terms and Conditions (https://onlinelibrary

on Wiley Online Library for rules of use; OA articles are gov

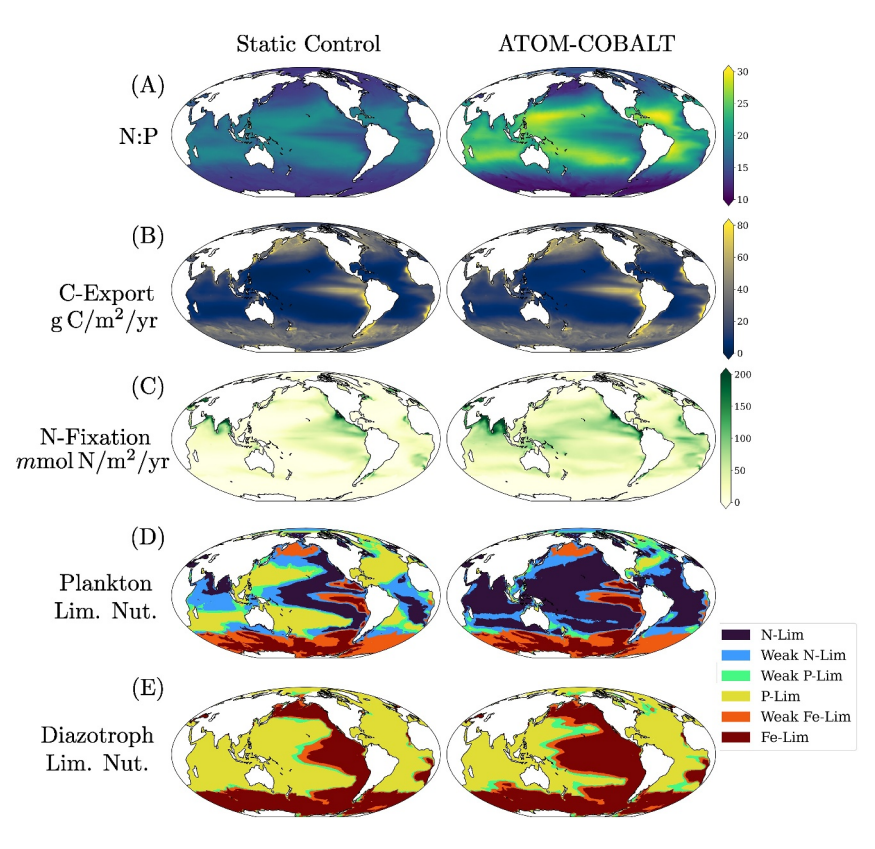


**Figure 4.** Last 5 years of simulation results from the static and dynamic models, comparing N:P of exported particulate organic matter, total exported particulate organic carbon, water column nitrogen fixation, and nutrient limitation of small phytoplankton and diazotrophs.

All dynamic stoichiometry models produced qualitatively similar "first order" biogeographic patterns, with elevated N:P in oligotrophic gyres and reduced N:P in high-latitude and productive mid- and low-latitude regions (Figure 5 and Table 4). The growth rate model and frugal model, however, exhibited distinct second order patterns (Figures 5b and 5d). The frugal model shows weaker gradients in N:P across low and mid latitude ecosystems, but has the largest shift from the mid to high latitudes, reflecting patterns of phosphate concentrations. In the growth rate model (and also the dynamic and dynamic with translation compensation models, which incorporate the growth rate hypothesis), the growth rate mechanism enhances N:P contrast between oligotrophic and eutrophic

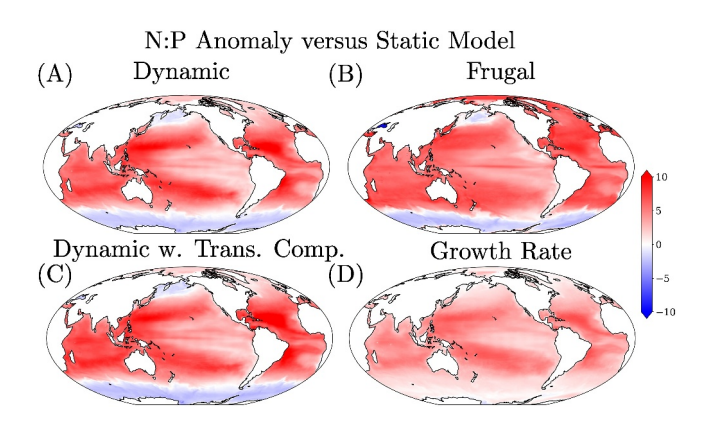


**Figure 5.** Difference of N:P ratios of exported organic matter between all dynamic stoichiometry models and static model (red means dynamic model had greater N:P) over the last 5 years of model simulations.

ecosystems, but has a weaker impact in high-latitude ecosystems. Figure S5 in Supporting Information S1 directly shows the difference in N:P ratios between the frugality and growth rate models. The frugal model produces higher N:P in oligotrophic gyres and in productive regions without excessive P, primarily productive regions that are not HNLC. The growth rate model has higher N:P ratios in HNLC areas, where luxury-P storage is at its greatest. The dynamic model and the dynamic model with translation compensation implement both the growth rate and frugality mechanisms and show both greater and more consistent N:P gradients between biomes than either the growth rate or frugal model. All models produce higher N:P ratios than the static control in low- and mid-latitude biomes, but in the high-latitudes biome the N:P ratios of all alternative models are closer to the controls and the static and translation-compensation model have lower N:P (Table 4).

These shifts in N:P ratios across models drive divergent biogeochemical outcomes: N-fixation (Figure 7) and export (Figure 8) increase in all alternative models, with the largest increase in the frugal model and the smallest in the growth rate model. Nitrogen fixation increased by 100% in the dynamic

HAGSTROM ET AL. 15 of 23

19449224, 2024, 5, Downloaded from https://agupubs

onlinelibrary.wiley.com/doi/10.1029/2023GB007991 by Princeton University, Wiley Online Library on [23/07/2024]. See the Terms and Cond

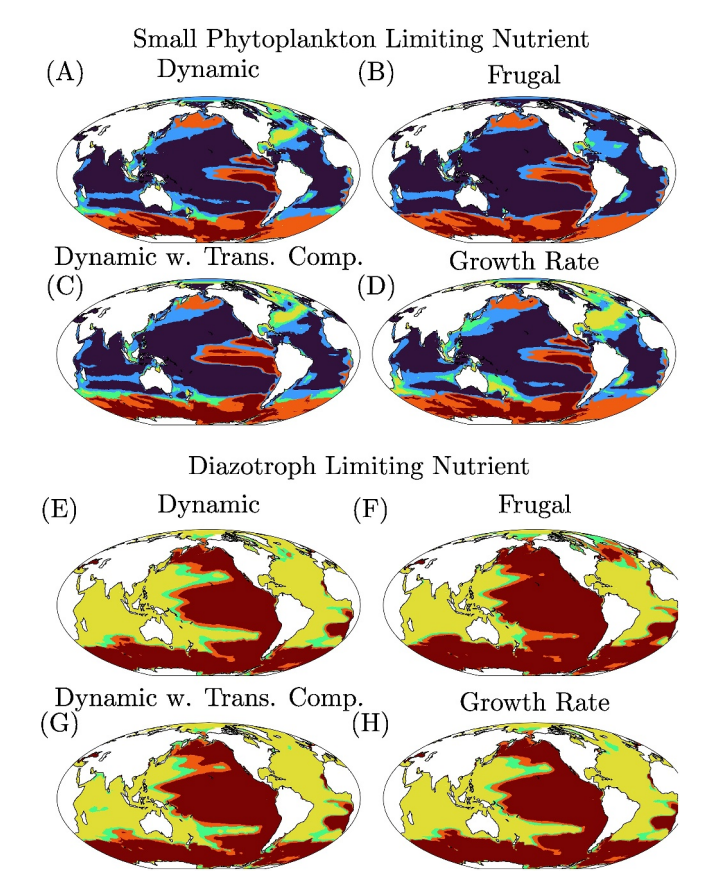


**Figure 6.** Nutrient limitation of primary productivity in small phytoplankton (top half) and diazotrophs (bottom half), across all dynamic model simulations. Right hand column shows global areal extent of different types of nutrient limitation.

model, 85% in the growth rate model, 153% in the frugal model, and 110% in the translation compensation model (Table 3). Carbon export followed trends in nitrogen fixation, increasing by 0.74 PgC/yr in the dynamic and growth-rate models, 1.13 PgC/yr in the frugal model, and 1.05 PgC/yr in the translation compensation model (Table 5). The magnitude of nitrogen fixation in each simulation corresponds to the magnitude of N:P ratios, and in particular the frugal model generated both high N:P ratios and high nitrogen fixation rates in low- and mid-latitude productive regions, suggesting that reductions in cellular P-quotas caused in ecosystems where P is low but non-limiting increases the niche size for diazotrophs. Conversely, less efficient P-utilization in the growth-rate model decreases nitrogen fixation in the low-P Atlantic and Indian oceans as well as the western Pacific subtropical gyre.

Higher N:P ratios (partially mitigated by increases in N-fixation) manifested in declines in the areal extent of P-limitation across the simulations for bulk phytoplankton where the area declined from 30% in the static model to 8% in the dynamic model, 12% in the growth rate model, 2% in the frugal model, and 10% in the dynamic with translation compensation model (Figure 6 and Table 6). Diazotroph nutrient limitation patterns also shifted, declining from 63% P-limited in the static control to 51% in the dynamic model, 51% in the growth rate model, 39% in the frugal model and 49% in the dynamic with translation compensation model. N:P dynamics due to both growth rate and frugal P utilization drove large declines in P-limitation, but the suppression of P-limitation in the frugality model was strongest, due to decreased P-export in ecosystems with low but non-limiting P in those simulations.

The dynamic model with translation compensation caused quantitatively similar biogeographic patterns to the dynamic model, despite the two models predicting strongly different N:P ratios across a temperature gradient in otherwise static environmental conditions (Figure S3 in Supporting Information S1). Translation compensation causes the optimal ratio of biosynthetic to photosynthetic machinery (E:L) to decrease with temperature (Equations S2 and S4 in Supporting Information S1), making N:P increase with tem-

perature. However, translation compensation also reduces the temperature dependence of phytoplankton maximum growth rates due to the decreased E:L at higher temperatures, which leads to smaller investments in E at maximum growth rates. This resulted in interactive effects which decreased the impact of temperature on realized N:P, N-fixation, and export. Further, in the case of carbon export from the Southern Ocean and other HNLC regions, the temperature impact was the reverse of expectations (Figure 8c). We explore this effect in greater detail in Text S3 of the Supporting Information S1 and revisit in the Discussion.

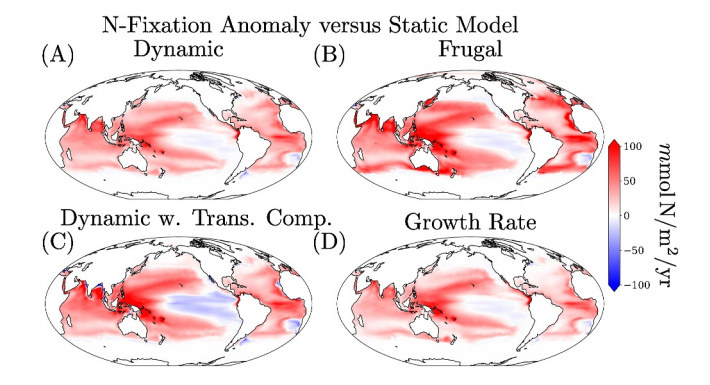


**Figure 7.** Differences between water column nitrogen fixation rates in dynamic model simulations and the static model averaged over the last 5 years of simulations.

### 4. Discussion

Here we showed that the dynamics of phytoplankton elemental stoichiometry have fundamental impacts on global-scale nutrient limitation patterns, N-fixation, and carbon export. This impact arises because phytoplankton stoichiometry determines how strongly phytoplankton couple elemental cycles. We developed a new model framework called ATOM-COBALT which captures the global biogeography of phytoplankton N:P and used it to show that under dynamic stoichiometry the ocean exhibits reduced P-limitation and increased N-fixation rates. Dynamic stoichiometry allows for greater variation of N:P, decreasing P-utilization across low-latitude regions, and in particular P-deplete regions such as the subtropical North Atlantic or coastal regions near high anthropogenic N-inputs, leading to a decline in P-limitation and greater availability of P for diazotrophs. Resource ratio theory and the Redfield paradigm suggest that when the N:P of inorganic nutrient supply is lower than the N:P of phytoplankton, there is a niche for diazotrophs which

HAGSTROM ET AL. 16 of 23

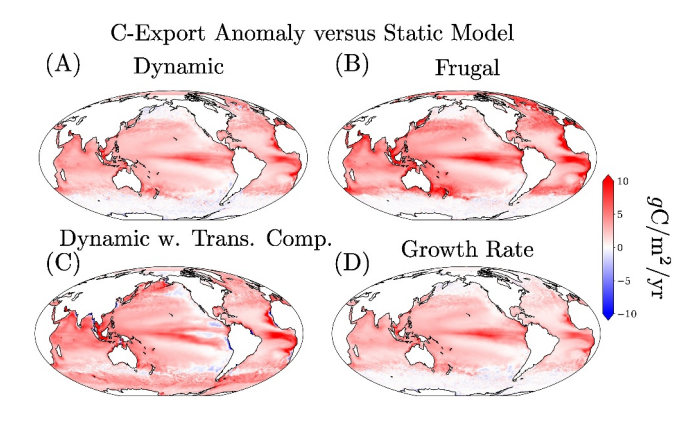


**Figure 8.** Differences between carbon export between dynamical model simulations and the static model averaged over the last 5 years of simulations. Right hand column shows globally integrated anomalies.

add new N and deplete available P (Lenton & Watson, 2000). Higher N:P in oligotrophic ecosystems therefore increases the size of the niche for diazotrophs, causing increased N-fixation and ultimately export compared to static ratios.

Phytoplankton frugality, the growth rate mechanism, and translation compensation each provide a physiological mechanism that quantitatively explains observed N:P ratios (Galbraith & Martiny, 2015; Klausmeier et al., 2004; Yvon-Durocher et al., 2015), however, these mechanisms can also cause ecosystem functions to have different sensitivity to environmental drivers and lead to different biogeochemical outcomes. Although our results here do not select one mechanism over another, they do elucidate the impacts of each mechanism for biogeographic patterns of N:P, nutrient limitation, N-fixation, and export. The frugality and growth rate mechanisms cause different responses to concentrations of non-limiting nutrients. Non-limiting nutrient concentrations do not impact growth rate and thus have no effect on the contribution of the growth rate mechanism to N:P in any model. On the

other hand, frugality causes N:P to increase whenever P decreases, whether or not P limits phytoplankton. This resulted in more P-availability in the frugal model, and less in the growth rate model, decreasing P limitation and increasing both N-fixation and carbon export in the frugal model compared with all other models.

Although the growth rate and frugality mechanisms produced qualitatively similar biogeographic patterns, the enhanced N:P ratios that occur in productive ecosystems under frugality alone caused large differences in N-fixation patterns and both total N-fixation and C-export. N:P observations cannot yet fully disentangle these distinct mechanisms, and models using frugality (or other single factors) alone can reproduce the lowest order global distribution of N:P ratios when fit to data. Our simulations provide some evidence that the frugal model is partially aliasing stoichiometric patterns driven by variations in N:P ratios driven by the growth mechanism, and the high N:P produced by the frugal model in low- and mid-latitude eutrophic ecosystems and the sub-polar North Atlantic suggest that the growth rate mechanism is needed to fully capture the dynamics of phytoplankton N:P and their implications for biogeochemistry. More observations of N:P and comparisons with simulation are needed to fully resolve this issue.

Several studies have identified a positive relationship between temperature and phytoplankton N:P (Martiny, Pham, et al., 2013; Yvon-Durocher et al., 2015), leading to suggestions that temperature driven changes in N:P will moderate expected declines in export in response to anthropogenic warming (Martiny, Hagstrom, et al., 2022; Moreno et al., 2018). Adding translation compensation to the dynamic model showed only very modest shifts in N:P and export. The deviation of the dynamic model with translation compensation simulation from our expectations based solely on N:P ratios may have been caused by shifts in the functional response of phytoplankton to temperature under translation compensation.

Under translation compensation, the kinetics of the photosynthetic machinery do not change with temperature (achieved by setting  $\kappa_{photo}=0$ ), which leads to cell growth rates exhibiting a flatter temperature dependence (see Figure S2 in Supporting Information S1), because the rate coefficients of both the biosynthetic and photosynthetic compartments contribute to the overall cell growth rate. This altered dependence increases the competitive abilities of phytoplankton in cold waters and decreases them in warm waters, with the discrepancy between the

 Table 4

 Mean Export N:P of Alternative Models in Different Ocean Biomes and Discrepancy From Static Control Model

Model	Global	Oligotrophic	Low-lat HC	Mic-lat HC	High lat
Static Control	14.9	18.3	16.4	15.9	13.6
ATOM-COBALT	16.4 (+1.5)	24.2 (+5.9)	19.2 (+2.8)	19.9 (+4.0)	13.1 (-0.5)
Growth Rate	16.2 (+1.3)	22.8 (+4.5)	18.6 (+2.2)	18.7 (+2.8)	14.3 (+0.7)
Frugal	17.6 (+2.7)	23.9 (+5.6)	20.2 (+3.8)	20.8 (+4.9)	14.1 (+0.5)
Dynamic w. Trans. Comp.	16.7 (+1.8)	24.5 (+6.2)	20.1 (+3.7)	19.9 (+4.0)	12.7 (-0.9)

HAGSTROM ET AL. 17 of 23

19449224, 2024, 5, Downloaded from https://agupubs.onlinelibrary.wiley.com/doi/10.1029/2023GB007991 by Princeton University, Wiley Online Library on [23/07/2024]. See the Terms and Cond

**Table 5**Globally Integrated Carbon Export in the Static Control Model, the Dynamic Model, and All Alternative Models

Model	Global export (PgC/yr)
Static Control	7.5
Dynamic	8.2 (0.7)
Growth Rate	8.2 (0.7)
Frugal	8.6 (1.1)
Dynamic w. Trans. Comp.	8.5 (1.0)

Note. Anomaly from static control reported in parentheses.

two models greatest when light and nutrients are abundant. The increased growth rate of phytoplankton in cold waters caused the translation compensation model to generate higher export from high-latitude ecosystems despite the reduced N:P ratios there (Figure 8c). Thus, the contrasting effect of translation compensation on growth rates and N:P make it unclear how this mechanism would affect biogeochemistry in a warmer or colder ocean (e.g., under anthropogenic warming or a glacial/interglacial transition), which are important questions that requires further study. The outcome of the dynamic with translation compensation model also shows the importance of using mechanistic models within self-consistent, biogeochemical simulations, as the result was dependent on how the temperature dependence of biochemical processes in the cell impact different organism level functional responses (e.g., comparing to the box-model based studies of translation-compensation in Moreno et al. (2018)).

Our simulations are consistent with both field observations that show mean phytoplankton N:P ratios (21:1 (Tanioka, Larkin, et al., 2022)) exceed the traditional Redfield ratio and global hydrographic observations which show that below the surface nitrate and phosphate concentrations scatter around a 16:1 regression line (Sarmiento & Gruber, 2006). Although N:P ratios exceed Redfield throughout most of the ocean, export in the ocean is skewed to regions with lower N:P ratios which causes the ratio of total exported PON to total exported POP to fall below the mean N:P of phytoplankton. It has been hypothesized (Redfield, 1958; Tyrrell, 1999) that the Redfield ratio is an optimal or even fundamental aspect of phytoplankton physiology, leading to homeostatic control of marine nitrogen cycling, but observations showing a significant deviations away from this ratio (DeVries & Deutsch, 2014; Martiny, Pham, et al., 2013; Tanioka, Larkin, et al., 2022; Teng et al., 2014) suggests that the emergence of the Redfield ratio and the ultimate regulation of the nitrogen cycle is more complex.

The qualitative distribution of macronutrients and nitrogen fixation of the dynamic N:P simulation is analogous to that of TOPAZ, the biogeochemical model part of GFDL's ESM2M and ESM2G, which included a dynamic N:P formulation (J. P. Dunne et al., 2013). TOPAZ implemented aspects of the growth rate mechanism through varying allocations to ribosomes following Klausmeier et al. and elements of frugality through luxury phosphorus uptake, only in the large phytoplankton size class. Here, we have significantly advanced previous formulations by taking advantage of improved global data sets and understanding of the physiological mechanisms and quantitative allocations that contribute to cellular N:P ratios (Daines et al., 2014; C. A. Garcia et al., 2020; Moreno et al., 2018). While there are numerous differences between TOPAZ and ATOM-COBALT, TOPAZ simulations produced robust global nitrogen fixation levels similar to those seen in our dynamic model. As shown in our results, such a response can emerge from both growth and frugality dynamics, suggesting that the formulation differences do not fundamentally shift this basic response. Similarly, several other dynamic N:P formulations

**Table 6**Global Fractions of Nutrient Limitation of Small Phytoplankton and Diazotrophs in the Static Control Model, Dynamic Model, and All Alternative Models

Model	N-Lim	P-Lim	Fe-Lim
Static Control Phyto.	0.41	0.23	0.36
Dynamic Phyto.	0.68	0.24	0.08
Growth Rate Phyto.	0.62	0.25	0.13
Frugal Phyto.	0.73	0.25	0.02
Dynamic w. Trans. Comp. Pyto.	0.65	0.25	0.10
Static Control Diazo.		0.37	0.63
Dynamic Diazo.		0.49	0.51
Growth Rate Diazo.		0.49	0.51
Frugal Diazo.		0.61	0.39
Dynamic w. Trans. Comp. Diazo.		0.51	0.49

which use empirical relationships to predict N:P from environmental conditions also achieve comparable large-scale macronutrient distributions, robust nitrogen fixation patterns, and resilience to excess P limitation (Bopp et al., 2022; Kwiatkowski et al., 2020; Kwon et al., 2022; Tagliabue et al., 2021).

#### 4.1. Model Limitations

The ATOM-COBALT model framework has several key limitations. In order to harmonize ATOM and COBALT, we had to simplify ATOM and adapt it to the two size class structure of COBALT. The cell radius trait impacts ATOM's predicted N:P ratios and also enables calculation of a single optimal strategy in all environmental conditions. Predicted N:P in ATOM-COBALT thus depends on both the food-web dynamics, which sets the balance between small and large phytoplankton, but also on the ATOM implementation within each size class which includes an implicit assignment of a cell radius to each type. Model tuning used the original ATOM parameters as a starting point and was adjusted using idealized, zero-D food web simulations to ensure that each size class produced a range of N:P consistent with observations. ATOM-

HAGSTROM ET AL. 18 of 23

COBALT could be improved through a model-fitting procedure that used simulations and incorporated additional observations beyond N:P ratios, however this is a computationally and conceptually challenging task that will be taken up in future work. ATOM-COBALT also assumes that phytoplankton C:N ratios are static. Greater plasticity of N:P compared with C:N (Sterner & Elser, 2017; Tanioka, Larkin, et al., 2022) and the existence of several mechanistic explanations for N:P variations (Klausmeier et al., 2004; Moreno & Martiny, 2018) provided justification for this assumption. However, systematic C:N variations increasingly appear in observations (Martiny, Vrugt, et al., 2013; Tanioka, Garcia, et al., 2022; Tanioka, Larkin, et al., 2022) and C:N variation may be an important biogeochemical driver (Inomura et al., 2022). Assuming static C:N could cause biases compared with observations in certain ocean regions where C:N shows greater variation. For instance, the recent GO-SHIP P18 (Lee et al., 2021), IO9N (C. A. Garcia et al., 2018), and IO7N (Tanioka, Garcia, et al., 2022) expeditions all observed regions of relatively muted N:P variations combined with enhanced C:N variations. Incorporating dynamic phytoplankton C:N requires better understanding of the physiological and environmental drivers behind its variation.

#### 4.2. Global Implications and Conclusions

Our results have implications for our understanding of how the oceans will respond to anthropogenic perturbations such as global warming or eutrophication. Increasing stratification is expected to reduce nutrient supplies to the surface ocean, leading to declines in productivity, export, and phytoplankton biomass, which are also predicted to limit the carbon available for higher trophic levels (Bopp et al., 2013). Dynamic N:P provides a mechanism for phytoplankton productivity, biomass, and export to be more resilient to declines in nutrient supply, through the more efficient use of P in oligotrophic ecosystems increasing export. We saw this increased resilience in the dynamic N:P simulations where productivity and export were enhanced in the subtropical gyres compared to the static control. These results are consistent with estimates from inverse models (DeVries & Deutsch, 2014; Teng et al., 2014), oxygen utilization in the thermocline (Emerson, 2014), and an emerging perspective of phytoplankton resilience to oligotrophic conditions (Martiny, Hagstrom, et al., 2022). Some model simulations which incorporate greater phytoplankton flexibility show a muted (Bopp et al., 2022; Kwiatkowski et al., 2020; Tagliabue et al., 2021) or even reversed (Kwon et al., 2022) (increased NPP under warming) response of the carbon cycle to future conditions. Together, these results suggest that changes in phytoplankton stoichiometry buffer productivity and carbon export against the effects of ocean warming.

The reduction of P-limitation under dynamic N:P could change the sensitivity of the carbon cycle to nutrient additions. Anthropogenic N-inputs can increase productivity in coastal regions (Rabalais et al., 2002), but in static simulations, particularly with N:P ratios as chosen in ESM4.1, these areas rapidly transition to P-limitation, limiting the potential impact on productivity. Together with the lack of observed P-limitation, this suggests that models with static N:P may underestimate the productivity response to increased external nutrient additions. In dynamic simulations, increases in the N:P ratio allows for N-limitation to persist at much higher resource supply ratios, which may cause more rapid uptake of externally supplied nutrients. Eutrophication of coastal waters and the subsequent expansion of hypoxic and anoxic regions have been a consequence of increased industrialization and are predicted to accelerate in a warming ocean, due to a combination of stratification, reduced oxygen saturation at the surface, and increased respiration in warmer waters (Penn & Deutsch, 2022; Rabalais et al., 2002). By better resolving nutrient limitation patterns, dynamic simulations can improve predictions of how phytoplankton mediate the interactions between eutrophication, deoxygenation, and warming. Declines in Plimitation also extended to diazotrophs in dynamic simulations, leading to a balance between areas of P- and Fe-limitation. Over long time scales, the supply rate of the nutrient limiting diazotrophs exerts strong controls on the nitrogen cycle and ultimately primary productivity (Redfield, 1958). Phytoplankton N:P helps determine these nutrient limitation patterns and thus is essential for modeling biogeochemistry at global scales. Capturing longterm N-cycle feedbacks has been a challenge in ESMs, and the large increase in N-fixation triggered by dynamic N:P confirms theoretical work suggesting these ratios are critical for modeling the N-cycle.

Our findings here reinforce the idea that variations of phytoplankton elemental stoichiometry are key drivers of marine biogeochemical cycles. We also showed that it is important to reduce uncertainty about the physiological mechanisms that lead to variations in phytoplankton N:P as these mechanisms lead to different responses on both regional and global scales. Dynamic stoichiometry complicates the picture of global biogeochemical cycles built atop the Redfield paradigm, leading to both large-scale and subtle changes that emerge from phytoplankton

HAGSTROM ET AL. 19 of 23



# **Global Biogeochemical Cycles**

10.1029/2023GB007991

physiology and ecosystem dynamics. Going forward, we suggest tighter integration of laboratory and field studies of phytoplankton N:P with global biogeochemical modeling.

# **Data Availability Statement**

The observations of particulate organic matter stoichiometry and the computer code for the ATOM-COBALT model are available at https://zenodo.org/doi/10.5281/zenodo.10946750 (G. Hagstrom et al., 2024). Simulation data required to perform the analyses contained in this paper and generate the figures are stored in an online repository at https://zenodo.org/record/8393830 (G. Hagstrom et al., 2023).

#### Acknowledgments References

GIH and SAL acknowledge support from the U.S. Department of Commerce National Oceanic and Atmospheric Administration (NOAA Grant NA18OAR4320123) and the National Science Foundation (NSF Grant IOS 2137340), and a gift from William H. Miller III. JYL acknowledges support from the NOAA Marine Ecosystem Tipping Points initiative. We thank John Dunne and Elise Olson for comments that improved a previous version of this manuscript.

- Adcroft, A., Anderson, W., Balaji, V., Blanton, C., Bushuk, M., Dufour, C. O., et al. (2019). The GFDL global ocean and sea ice model OM4. 0: Model description and simulation features. *Journal of Advances in Modeling Earth Systems*, 11(10), 3167–3211. https://doi.org/10.1029/2019ps:001776
- Behrenfeld, M. J., Boss, E., Siegel, D. A., & Shea, D. M. (2005). Carbon-based ocean productivity and phytoplankton physiology from space. *Global Biogeochemical Cycles*, 19(1). https://doi.org/10.1029/2004gb002299
- Bopp, L., Aumont, O., Kwiatkowski, L., Clerc, C., Dupont, L., Ethé, C., et al. (2022). Diazotrophy as a key driver of the response of marine net primary productivity to climate change. *Biogeosciences*, 19(17), 4267–4285. https://doi.org/10.5194/bg-19-4267-2022
- Bopp, L., Resplandy, L., Orr, J. C., Doney, S. C., Dunne, J. P., Gehlen, M., et al. (2013). Multiple stressors of ocean ecosystems in the 21st century: Projections with CMIP5 models. *Biogeosciences*, 10, 6225–6245. https://doi.org/10.5194/bg-10-6225-2013
- Capone, D. G., Zehr, J. P., Paerl, H. W., Bergman, B., & Carpenter, E. J. (1997). Trichodesmium, a globally significant marine cyanobacterium. Science, 276(5316), 1221–1229. https://doi.org/10.1126/science.276.5316.1221
- Chien, C.-T., Pahlow, M., Schartau, M., Li, N., & Oschlies, A. (2023). Effects of phytoplankton physiology on global ocean biogeochemistry and climate. Science Advances, 9(30), eadg1725. https://doi.org/10.1126/sciadv.adg1725
- Daines, S. J., Clark, J. R., & Lenton, T. M. (2014). Multiple environmental controls on phytoplankton growth strategies determine adaptive responses of the N:P ratio. *Ecology Letters*, 17(4), 414–425. https://doi.org/10.1111/ele.12239
- Danabasoglu, G., Lamarque, J.-F., Bacmeister, J., Bailey, D., DuVivier, A., Edwards, J., et al. (2020). The community Earth system model version
- 2 (CESM2). Journal of Advances in Modeling Earth Systems, 12(2), e2019MS001916. https://doi.org/10.1029/2019ms001916

  Deutsch, C., & Weber, T. (2012). Nutrient ratios as a tracer and driver of ocean biogeochemistry. Annual Review of Marine Science, 4(1), 113–141. https://doi.org/10.1146/annurev-marine-120709-142821
- Devault, D. (1980). Quantum mechanical tunnelling in biological systems. Quarterly Reviews of Biophysics, 13(4), 387–564. https://doi.org/10.1017/s003358350000175x
- DeVries, T., & Deutsch, C. (2014). Large-scale variations in the stoichiometry of marine organic matter respiration. *Nature Geoscience*, 7(12), 890-894. https://doi.org/10.1038/nge02300
- Dunne, J., Horowitz, L., Adcroft, A., Ginoux, P., Held, I., John, J., et al. (2020). The GFDL Earth system model version 4.1 (GFDL-ESM 4.1):

  Overall coupled model description and simulation characteristics. *Journal of Advances in Modeling Earth Systems*, 12(11), e2019MS002015. https://doi.org/10.1029/2019ms002015
- Dunne, J. P., John, J. G., Shevliakova, E., Stouffer, R. J., Krasting, J. P., Malyshev, S. L., et al. (2013). GFDL's ESM2 global coupled climate–carbon Earth system models. Part II: Carbon system formulation and baseline simulation characteristics. *Journal of Climate*, 26(7), 2247–2267. https://doi.org/10.1175/jcli-d-12-00150.1
- Dunne, J. P., Sarmiento, J. L., & Gnanadesikan, A. (2007). A synthesis of global particle export from the surface ocean and cycling through the ocean interior and on the seafloor. *Global Biogeochemical Cycles*, 21(4). https://doi.org/10.1029/2006gb002907
- Elser, J., Sterner, R. W., Gorokhova, E., Fagan, W., Markow, T., Cotner, J. B., et al. (2000). Biological stoichiometry from genes to ecosystems. Ecology Letters, 3(6), 540–550. https://doi.org/10.1046/j.1461-0248.2000.00185.x
- Emerson, S. (2014). Annual net community production and the biological carbon flux in the ocean. *Global Biogeochemical Cycles*, 28(1), 14–28. https://doi.org/10.1002/2013gb004680
- Eppley, R. W. (1972). Temperature and phytoplankton growth in the sea. Fishery Bulletin, 70(4), 1063-1085.
- Galbraith, E. D., & Martiny, A. C. (2015). A simple nutrient-dependence mechanism for predicting the stoichiometry of marine ecosystems. Proceedings of the National Academy of Sciences of the United States of America, 112(27), 8199–8204. https://doi.org/10.1073/pnas. 1423917112
- Garcia, C. A., Baer, S. E., Garcia, N. S., Rauschenberg, S., Twining, B. S., Lomas, M. W., & Martiny, A. C. (2018). Nutrient supply controls particulate elemental concentrations and ratios in the low latitude eastern Indian Ocean. *Nature Communications*, 9(1), 4868. https://doi.org/10.1038/s41467-018-06892-w
- Garcia, C. A., Hagstrom, G. I., Larkin, A. A., Ustick, L. J., Levin, S. A., Lomas, M. W., & Martiny, A. C. (2020). Linking regional shifts in microbial genome adaptation with surface ocean biogeochemistry. *Philosophical Transactions of the Royal Society B*, 375(1798), 20190254. https://doi.org/10.1098/rstb.2019.0254
- Garcia, H., Locarnini, R., Boyer, T., Antonov, J., Baranova, O., Zweng, M., et al. (2014). World Ocean Atlas 2013, volume 4: Dissolved inorganic nutrients (phosphate, nitrate, silicate). In S. Levitus (Ed.), NOAA Atlas NESDIS (Vol. 76, p. 25). US Government Printing Office.
- Garcia, H. E., Locarnini, R. A., Boyer, T. P., Antonov, J. I., Baranova, O. K., Zweng, M. M., et al. (2013). World Ocean Atlas 2013: Dissolved inorganic nutrients (phosphate, nitrate, silicate). US Department of Commerce, National Oceanic and Atmospheric Administration.
- Geider, R., MacIntyre, H., & Kana, T. (1997). Dynamic model of phytoplankton growth and acclimation: Responses of the balanced growth rate and the chlorophyll a: Carbon ratio to light, nutrient-limitation and temperature. *Marine Ecology Progress Series*, 148, 187–200. https://doi. org/10.3354/meps148187
- Großkopf, T., Mohr, W., Baustian, T., Schunck, H., Gill, D., Kuypers, M. M., et al. (2012). Doubling of marine dinitrogen-fixation rates based on direct measurements. *Nature*, 488(7411), 361–364. https://doi.org/10.1038/nature11338
- Hagstrom, G., Stock, C., Luo, J., & Levin, S. (2023). Simulation data for "impact of dynamic phytoplankton stoichiometry on global scale patterns of nutrient limitation, nitrogen fixation, and carbon export". Zenodo. https://doi.org/10.5281/zenodo.8393830

HAGSTROM ET AL. 20 of 23

- Hagstrom, G., Stock, C., Luo, J., & Levin, S. (2024). Software code for "impact of dynamic phytoplankton stoichiometry on global scale patterns of nutrient limitation, nitrogen fixation, and carbon export". Zenodo. https://doi.org/10.5281/zenodo.10946751
- Hagstrom, G. I., & Levin, S. A. (2017). Marine ecosystems as complex adaptive systems: Emergent patterns, critical transitions, and public goods. Ecosystems, 20(3), 458–476. https://doi.org/10.1007/s10021-017-0114-3
- Horowitz, L. W., Walters, S., Mauzerall, D. L., Emmons, L. K., Rasch, P. J., Granier, C., et al. (2003). A global simulation of tropospheric ozone and related tracers: Description and evaluation of MOZART, version 2. *Journal of Geophysical Research*, 108(D24), 4784. https://doi.org/10.1029/2002jd002853
- Inomura, K., Deutsch, C., Jahn, O., Dutkiewicz, S., & Follows, M. J. (2022). Global patterns in marine organic matter stoichiometry driven by phytoplankton ecophysiology. *Nature Geoscience*, 15(12), 1034–1040. https://doi.org/10.1038/s41561-022-01066-2
- Klausmeier, C. A., Litchman, E., Daufresne, T., & Levin, S. A. (2004). Optimal nitrogen-to-phosphorus stoichiometry of phytoplankton. *Nature*, 429(6988), 171–174. https://doi.org/10.1038/nature02454
- Kulk, G., Platt, T., Dingle, J., Jackson, T., Jönsson, B. F., Bouman, H. A., et al. (2020). Primary production, an index of climate change in the ocean: Satellite-based estimates over two decades. *Remote Sensing*, 12(5), 826. https://doi.org/10.3390/rs12050826
- Kwiatkowski, L., Aumont, O., Bopp, L., & Ciais, P. (2018). The impact of variable phytoplankton stoichiometry on projections of primary production, food quality, and carbon uptake in the global ocean. Global Biogeochemical Cycles, 32(4), 516–528. https://doi.org/10.1002/2017gb005799
- Kwiatkowski, L., Torres, O., Bopp, L., Aumont, O., Chamberlain, M., Christian, J. R., et al. (2020). Twenty-first century ocean warming, acidification, deoxygenation, and upper-ocean nutrient and primary production decline from CMIP6 model projections. *Biogeosciences*, 17(13), 3439–3470. https://doi.org/10.5194/bg-17-3439-2020
- Kwon, E. Y., Sreeush, M., Timmermann, A., Karl, D. M., Church, M. J., Lee, S.-S., & Yamaguchi, R. (2022). Nutrient uptake plasticity in phytoplankton sustains future ocean net primary production. *Science Advances*, 8(51), eadd2475, https://doi.org/10.1126/sciady.add2475
- Large, W., & Yeager, S. (2009). The global climatology of an interannually varying air–sea flux data set. Climate Dynamics, 33(2), 341–364. https://doi.org/10.1007/s00382-008-0441-3
- Lauvset, S. K., Key, R. M., Olsen, A., Van Heuven, S., Velo, A., Lin, X., et al. (2016). A new global interior ocean mapped climatology: The 1×1 GLODAP version 2. *Earth System Science Data*, 8(2), 325–340. https://doi.org/10.5194/essd-8-325-2016
- Lee, J. A., Garcia, C. A., Larkin, A. A., Carter, B. R., & Martiny, A. C. (2021). Linking a latitudinal gradient in ocean hydrography and elemental stoichiometry in the eastern Pacific Ocean. *Global Biogeochemical Cycles*, 35(5), e2020GB006622. https://doi.org/10.1029/2020gb006622
- Lenton, T. M., & Watson, A. J. (2000). Redfield revisited: 1. Regulation of nitrate, phosphate, and oxygen in the ocean. *Global Biogeochemical Cycles*, 14(1), 225–248. https://doi.org/10.1029/1999gb900065
- Litchman, E., & Klausmeier, C. A. (2008). Trait-based community ecology of phytoplankton. Annual Review of Ecology, Evolution, and Systematics, 39(1), 615–639. https://doi.org/10.1146/annurev.ecolsys.39.110707.173549
- Long, M. C., Moore, J. K., Lindsay, K., Levy, M., Doney, S. C., Luo, J. Y., et al. (2021). Simulations with the marine biogeochemistry library (MARBL). *Journal of Advances in Modeling Earth Systems*, 13(12), e2021MS002647. https://doi.org/10.1029/2021ms002647
- Luo, Y.-W., Doney, S., Anderson, L., Benavides, M., Berman-Frank, I., Bode, A., et al. (2012). Database of diazotrophs in global ocean: Abundance, biomass and nitrogen fixation rates. *Earth System Science Data*, 4(1), 47–73. https://doi.org/10.5194/essd-4-47-2012
- Martiny, A. C., Hagstrom, G. I., DeVries, T., Letscher, R. T., Britten, G. L., Garcia, C. A., et al. (2022). Marine phytoplankton resilience may moderate oligotrophic ecosystem responses and biogeochemical feedbacks to climate change. *Limnology & Oceanography*, 67(S1),
- S378–S389. https://doi.org/10.1002/lno.12029

  Martiny, A. C., Lomas, M. W., Fu, W., Boyd, P. W., Chen, Y.-L. L., Cutter, G. A., et al. (2019). Biogeochemical controls of surface ocean phosphate. *Science Advances*, 5(8), eaax0341. https://doi.org/10.1126/sciadv.aax0341
- Martiny, A. C., Pham, C. T., Primeau, F. W., Vrugt, J. A., Moore, J. K., Levin, S. A., & Lomas, M. W. (2013). Strong latitudinal patterns in the elemental ratios of marine plankton and organic matter. *Nature Geoscience*, 6(4), 279–283. https://doi.org/10.1038/ngeo1757
- Martiny, A. C., Vrugt, J. A., & Lomas, M. W. (2014). Concentrations and ratios of particulate organic carbon, nitrogen, and phosphorus in the global ocean. *Scientific Data*, 1, 140048. https://doi.org/10.1038/sdata.2014.48
- Martiny, A. C., Vrugt, J. A., Primeau, F. W., & Lomas, M. W. (2013). Regional variation in the particulate organic carbon to nitrogen ratio in the surface ocean. *Global Biogeochemical Cycles*, 27(3), 723–731. https://doi.org/10.1002/gbc.20061
- Matsumoto, K., Tanioka, T., & Rickaby, R. (2020). Linkages between dynamic phytoplankton c: N: P and the ocean carbon cycle under climate change. *Oceanography*, 33(2), 44–52. https://doi.org/10.5670/oceanog.2020.203
- Moore, J. K., Fu, W., Primeau, F., Britten, G. L., Lindsay, K., Long, M., et al. (2018). Sustained climate warming drives declining marine biological productivity. *Science*, 359(6380), 1139–1143. https://doi.org/10.1126/science.aao6379
- Moreno, A. R., Hagstrom, G. I., Primeau, F. W., Levin, S. A., & Martiny, A. C. (2018). Marine phytoplankton stoichiometry mediates nonlinear interactions between nutrient supply, temperature, and atmospheric CO<sub>2</sub>. Biogeosciences, 15(9), 2761–2779. https://doi.org/10.5194/bg-15-2761-2018
- Moreno, A. R., & Martiny, A. C. (2018). Ecological stoichiometry of ocean plankton. Annual Review of Marine Science, 10(1), 43–69. https://doi.org/10.1146/annurev-marine-121916-063126
- O'Neill, R., DeAngelis, D., Pastor, J., Jackson, B., & Post, W. (1989). Multiple nutrient limitations in ecological models. *Ecological Modelling*, 46(3–4), 147–163. https://doi.org/10.1016/0304-3800(89)90015-x
- Pahlow, M., Chien, C.-T., Arteaga, L. A., & Oschlies, A. (2020). Optimality-based non-Redfield plankton–ecosystem model (OPEM v1. 1) in UVic-ESCM 2.9–part 1: Implementation and model behaviour. *Geoscientific Model Development*, 13(10), 4663–4690. https://doi.org/10.5194/smd-13-4663-2020
- Penn, J. L., & Deutsch, C. (2022). Avoiding ocean mass extinction from climate warming. Science, 376(6592), 524–526. https://doi.org/10.1126/science.abe9039
- Polovina, J. J., Dunne, J. P., Woodworth, P. A., & Howell, E. A. (2011). Projected expansion of the subtropical biome and contraction of the temperate and equatorial upwelling biomes in the North Pacific under global warming. *ICES Journal of Marine Science*, 68(6), 986–995. https://doi.org/10.1093/icesjms/fsq198
- Purcell, E. M. (1977). Life at low Reynolds number. American Journal of Physics, 45(1), 3-11. https://doi.org/10.1119/1.10903
- Rabalais, N. N., Turner, R. E., & Wiseman Jr, W. J. (2002). Gulf of Mexico hypoxia, aka "The dead zone". Annual Review of Ecology and Systematics, 33(1), 235–263. https://doi.org/10.1146/annurev.ecolsys.33.010802.150513
- Raven, J. A., & Geider, R. J. (1988). Temperature and algal growth. New Phytologist, 110(4), 441–461. https://doi.org/10.1111/j.1469-8137.1988. tb00282.x
- Redfield, A. C. (1958). The biological control of chemical factors in the environment. American Scientist, 46(3), 205-221.

HAGSTROM ET AL. 21 of 23

- Rhee, G.-Y. (1974). Phosphate uptake under nitrate limitation by *scenedesmus* sp. and its ecological implications 1. *Journal of Phycology*, 10(4), 470–475. https://doi.org/10.1111/j.0022-3646.1974.00470.x
- Sarmiento, J. L., & Gruber, N. (2006). Ocean biogeochemical dynamics. Princeton University Press.
- Séférian, R., Berthet, S., Yool, A., Palmieri, J., Bopp, L., Tagliabue, A., et al. (2020). Tracking improvement in simulated marine biogeochemistry between CMIP5 and CMIP6. Current Climate Change Reports, 6(3), 95–119. https://doi.org/10.1007/s40641-020-00160-0
- Seitzinger, S. P., Harrison, J. A., Dumont, E., Beusen, A. H., & Bouwman, A. (2005). Sources and delivery of carbon, nitrogen, and phosphorus to the coastal zone: An overview of Global Nutrient Export from Watersheds (NEWS) models and their application. *Global Biogeochemical Cycles*, 19(4). https://doi.org/10.1029/2005gb002606
- Shuter, B. (1979). A model of physiological adaptation in unicellular algae. *Journal of Theoretical Biology*, 78(4), 519–552. https://doi.org/10.1016/0022-5193(79)90189-9
- Smith, S. L., Pahlow, M., Merico, A., & Wirtz, K. W. (2011). Optimality-based modeling of planktonic organisms. *Limnology & Oceanography*, 56(6), 2080–2094. https://doi.org/10.4319/lo.2011.56.6.2080
- Sterner, R. W., & Elser, J. J. (2017). Ecological stoichiometry. In Ecological stoichiometry. Princeton University Press.
- Stock, C. A., Dunne, J. P., Fan, S., Ginoux, P., John, J., Krasting, J. P., et al. (2020). Ocean biogeochemistry in GFDL's Earth system model 4.1 and its response to increasing atmospheric CO<sub>2</sub>. *Journal of Advances in Modeling Earth Systems*, 12(10), e2019MS002043. https://doi.org/10.1029/2019ms002043
- Stock, C. A., Dunne, J. P., & John, J. G. (2014). Global-scale carbon and energy flows through the marine planktonic food web: An analysis with a coupled physical-biological model. *Progress in Oceanography*, 120, 1–28. https://doi.org/10.1016/j.pocean.2013.07.001
- Tagliabue, A., Kwiatkowski, L., Bopp, L., Butenschön, M., Cheung, W., Lengaigne, M., & Vialard, J. (2021). Persistent uncertainties in ocean net primary production climate change projections at regional scales raise challenges for assessing impacts on ecosystem services. Frontiers in Climate, 149. https://doi.org/10.3389/fclim.2021.738224
- Talmy, D., Blackford, J., Hardman-Mountford, N. J., Dumbrell, A. J., & Geider, R. J. (2013). An optimality model of photoadaptation in contrasting aquatic light regimes. *Limnology & Oceanography*, 58(5), 1802–1818. https://doi.org/10.4319/lo.2013.58.5.1802
- Tang, W., Wang, S., Fonseca-Batista, D., Dehairs, F., Gifford, S., Gonzalez, A. G., et al. (2019). Revisiting the distribution of oceanic N<sub>2</sub> fixation and estimating diazotrophic contribution to marine production. *Nature Communications*, 10(1), 1–10. https://doi.org/10.1038/s41467-019-08640-0
- Tanioka, T., Garcia, C. A., Larkin, A. A., Garcia, N. S., Fagan, A. J., & Martiny, A. C. (2022). Global patterns and predictors of C:N:P in marine ecosystems. *Communications Earth & Environment*, 3(1), 271. https://doi.org/10.1038/s43247-022-00603-6
- Tanioka, T., Larkin, A. A., Moreno, A. R., Brock, M. L., Fagan, A. J., Garcia, C. A., et al. (2022). Global ocean particulate organic phosphorus, carbon, oxygen for respiration, and nitrogen (GO-POPCORN). Scientific Data, 9(1), 688. https://doi.org/10.1038/s41597-022-01809-1
- Tanioka, T., & Matsumoto, K. (2017). Buffering of ocean export production by flexible elemental stoichiometry of particulate organic matter. Global Biogeochemical Cycles, 31(10), 1528–1542. https://doi.org/10.1002/2017gb005670
- Teng, Y.-C., Primeau, F. W., Moore, J. K., Lomas, M. W., & Martiny, A. C. (2014). Global-scale variations of the ratios of carbon to phosphorus in exported marine organic matter. *Nature Geoscience*, 7(12), 895–898. https://doi.org/10.1038/ngeo2303
- Toseland, A., Daines, S. J., Clark, J. R., Kirkham, A., Strauss, J., Uhlig, C., et al. (2013). The impact of temperature on marine phytoplankton resource allocation and metabolism. *Nature Climate Change*, 3(11), 979–984. https://doi.org/10.1038/nclimate1989
- Tyrrell, T. (1999). The relative influences of nitrogen and phosphorus on oceanic primary production. *Nature*, 400(6744), 525–531. https://doi.org/10.1038/22941
- Van Mooy, B. A., Rocap, G., Fredricks, H. F., Evans, C. T., & Devol, A. H. (2006). Sulfolipids dramatically decrease phosphorus demand by picocyanobacteria in oligotrophic marine environments. *Proceedings of the National Academy of Sciences of the United States of America*, 103(23), 8607–8612. https://doi.org/10.1073/pnas.0600540103
- von Liebig, J. (1840). Die organische Chemie in ihrer Anwendung auf Agricultur und Physiologie. Vieweg.
- Wang, W.-L., Moore, J. K., Martiny, A. C., & Primeau, F. W. (2019). Convergent estimates of marine nitrogen fixation. *Nature*, 566(7743), 205–211. https://doi.org/10.1038/s41586-019-0911-2
- Yvon-Durocher, G., Dossena, M., Trimmer, M., Woodward, G., & Allen, A. P. (2015). Temperature and the biogeography of algal stoichiometry. Global Ecology and Biogeography, 24(5), 562–570. https://doi.org/10.1111/geb.12280
- Zhao, M., Golaz, J.-C., Held, I., Guo, H., Balaji, V., Benson, R., et al. (2018). The GFDL global atmosphere and land model AM4. 0/LM4. 0: 2. Model description, sensitivity studies, and tuning strategies. *Journal of Advances in Modeling Earth Systems*, 10(3), 735–769. https://doi.org/10.1002/2017ms001209

### **References From the Supporting Information**

- Baer, S. E., Lomas, M. W., Terpis, K. X., Mouginot, C., & Martiny, A. C. (2017). Stoichiometry of *Prochlorococcus, Synechococcus*, and small eukaryotic populations in the western North Atlantic Ocean. *Environmental Microbiology*, 19(4), 1568–1583. https://doi.org/10.1111/1462-2920.13672
- Baker, A. R., & Croot, P. L. (2010). Atmospheric and marine controls on aerosol iron solubility in seawater. *Marine Chemistry*, 120(1–4), 4–13. https://doi.org/10.1016/j.marchem.2008.09.003
- Bode, A., Varela, M. M., Teira, E., Fernández, E., González, N., & Varela, M. (2004). Planktonic carbon and nitrogen cycling off northwest Spain: Variations in production of particulate and dissolved organic pools. *Aquatic Microbial Ecology*, 37(1), 95–107. https://doi.org/10.3354/ame037095
- Charpy, L., Dufour, P., & Garcia, N. (1997). Particulate organic matter in sixteen Tuamotu atoll lagoons (French Polynesia). *Marine Ecology Progress Series*, 151, 55–65. https://doi.org/10.3354/meps151055
- Clemente, T. M., Ernst, J., Fong, A., Updyke, B., Viviani, D., Weersing, K., et al. (2010). SUPER HI-CAT: Survey of underwater plastic and ecosystem response between Hawaii and California. In *Proceedings from the 2010 AGU ocean sciences meeting*.
- Copin-Montegut, C., & Copin-Montegut, G. (1978). The chemistry of particulate matter from the south Indian and Antarctic oceans. *Deep-Sea Research*, 25(10), 911–931. https://doi.org/10.1016/0146-6291(78)90633-1
- Copin-Montegut, C., & Copin-Montegut, G. (1983). Stoichiometry of carbon, nitrogen, and phosphorus in marine particulate matter. Deep-Sea Research, Part A: Oceanographic Research Papers, 30(1), 31–46. https://doi.org/10.1016/0198-0149(83)90031-6
- Dietze, H., Oschlies, A., & Kähler, P. (2004). Internal-wave-induced and double-diffusive nutrient fluxes to the nutrient-consuming surface layer in the oligotrophic subtropical North Atlantic. *Ocean Dynamics*, 54, 1–7. https://doi.org/10.1007/s10236-003-0060-9

HAGSTROM ET AL. 22 of 23

- Fichaut, M., Garcia, M., Giorgetti, A., Iona, A., Kuznetsov, A., Rixen, M., & Group, M. (2003). MEDAR/MEDATLAS 2002: A Mediterranean and Black Sea database for operational oceanography. In *Elsevier oceanography series* (Vol. 69, pp. 645–648). Elsevier. https://doi.org/10.1016/s0422-9894(03)80107-1
- Garcia, N. S., Talmy, D., Fu, W.-W., Larkin, A. A., Lee, J., & Martiny, A. C. (2022). The diel cycle of surface ocean elemental stoichiometry has implications for ocean productivity. *Global Biogeochemical Cycles*, 36(3), e2021GB007092. https://doi.org/10.1029/2021gb007092
- Gasol, J. M., Vázquez-Domínguez, E., Vaqué, D., Agustí, S., & Duarte, C. M. (2009). Bacterial activity and diffusive nutrient supply in the oligotrophic Central Atlantic Ocean. Aquatic Microbial Ecology, 56(1), 1–12. https://doi.org/10.3354/ame01310
- Hewson, I., Paerl, R. W., Tripp, H. J., Zehr, J. P., & Karl, D. M. (2009). Metagenomic potential of microbial assemblages in the surface waters of the central Pacific Ocean tracks variability in oceanic habitat. *Limnology & Oceanography*, 54(6), 1981–1994. https://doi.org/10.4319/lo.2009.
- Karl, D. M., Björkman, K. M., Dore, J. E., Fujieki, L., Hebel, D. V., Houlihan, T., et al. (2001). Ecological nitrogen-to-phosphorus stoichiometry at station ALOHA. Deep Sea Research Part II: Topical Studies in Oceanography, 48(8–9), 1529–1566. https://doi.org/10.1016/s0967-0645 (00)00152-1
- Larkin, A., Lee, J. A., & Martiny, A. C. (2020). POC, PON, and POP from surface underway water samples collected during AMT28/JR18001. (Technical Report). British Oceanographic Data Centre, National Oceanography Centre. https://doi.org/10.5285/d76d90bb-5d7a-5415-e053-6c86abc0d182
- Loh, A. N., & Bauer, J. E. (2000). Distribution, partitioning and fluxes of dissolved and particulate organic C, N and P in the eastern North Pacific and Southern Oceans. *Deep Sea Research Part I: Oceanographic Research Papers*, 47(12), 2287–2316. https://doi.org/10.1016/s0967-0637
- Lomas, M. W., Baer, S. E., Mouginot, C., Terpis, K. X., Lomas, D. A., Altabet, M. A., & Martiny, A. C. (2021). Varying influence of phyto-plankton biodiversity and stoichiometric plasticity on bulk particulate stoichiometry across ocean basins. *Communications Earth & Environment*, 2(1), 143. https://doi.org/10.1038/s43247-021-00212-9
- Lomas, M. W., Burke, A., Lomas, D., Bell, D., Shen, C., Dyhrman, S. T., & Ammerman, J. W. (2010). Sargasso Sea phosphorus biogeochemistry: An important role for dissolved organic phosphorus (DOP). *Biogeosciences*, 7(2), 695–710. https://doi.org/10.5194/bg-7-695-2010
- Lomas, M. W., & Martiny, A. C. (2020a). Depth profile data from R/V Atlantic explorer AE1319 in the NW Atlantic from Aug-Sept. 2013 (version 1) [Dataset] (Technical Report). Biological and Chemical Oceanography Data Management Office (BCO-DMO). https://doi.org/10. 26008/1912/BCO-DMO.829797.1
- Lomas, M. W., & Martiny, A. C. (2020b). Depth profle data from Bermuda Atlantic time-series validation cruise 46 (BVAL46) in the Sargasso Sea from Sept-Oct. 2011 (Technical Report). Biological and Chemical Oceanography Data Management Office (BCO-DMO). https://doi.org/ 10.26008/1912/bco-dmo.829843.1
- Lomas, M. W., & Martiny, A. C. (2020c). Depth profle data from R/V new horizons NH1418 in the tropical Pacific from Sept-Oct 2014 (Technical Report). Biological and Chemical Oceanography Data Management Office (BCO-DMO). https://doi.org/10.26008/1912/bco-dmo.829895.1
- Martiny, A. C., Garcia, C. A., Lee, J. A., Moreno, A. R., & Larkin, A. A. (2020). POM concentrations for carbon, nitrogen, phosphorus, and chemical oxygen from GO-SHIP Line P18 Legs 1 and 2 in 2016 and 2017 (Technical Report). Biological and Chemical Oceanography Data Management Office (BCO-DMO). https://doi.org/10.26008/1912/bco-dmo.816347.1
- Martiny, A. C., Garcia, C. A., Moreno, A. R., & Tanioka, T. (2022). POM concentrations for carbon, nitrogen, and phosphorus from GO-SHIP line I07N RB1803 in the western Indian Ocean from April to June 2018 (ocean stoichiometry Project) (Technical Report). Biological and Chemical Oceanography Data Management Office (BCO-DMO). https://doi.org/10.26008/1912/bco-dmo.879076.1
- Martiny, A. C., & Lomas, M. W. (2021). Particulate organic matter (PON, POC, POP) concentrations collected on R/V Roger Revelle cruise RR1604 along the hydrographic line IO9 in the eastern Indian Ocean from March to April 2016 (Technical Report). Biological and Chemical Oceanography Data Management Office (BCO-DMO). https://doi.org/10.26008/1912/bco-dmo.734915.3
- Moreno, A. R., Garcia, C. A., Larkin, A. A., Lee, J. A. A., Wang, W.-L., Moore, J. K., et al. (2020). Latitudinal gradient in the respiration quotient and the implications for ocean oxygen availability. *Proceedings of the National Academy of Sciences of the United States of America*, 117(37), 22866–22872. https://doi.org/10.1073/pnas.2004986117
- Moreno, A. R., Larkin, A. A., Lee, J. A., Gerace, S. D., Tarran, G. A., & Martiny, A. C. (2022). Regulation of the respiration quotient across ocean basins. *AGU Advances*, 3(5), e2022AV000679. https://doi.org/10.1029/2022av000679
- Moutin, T., Karl, D. M., Duhamel, S., Rimmelin, P., Raimbault, P., Van Mooy, B. A., & Claustre, H. (2008). Phosphate availability and the ultimate control of new nitrogen input by nitrogen fixation in the tropical Pacific Ocean. *Biogeosciences*, 5(1), 95–109. https://doi.org/10.5194/be-5-95-2008
- Passow, U., & Peinert, R. (1993). The role of plankton in particle flux: Two case studies from the northeast Atlantic. *Deep Sea Research Part II:* Topical Studies in Oceanography, 40(1–2), 573–585. https://doi.org/10.1016/0967-0645(93)90033-j
- Rodier, M., & Le Borgne, R. (1997). Export flux of particles at the equator in the western and central Pacific Ocean. *Deep Sea Research Part II: Topical Studies in Oceanography*, 44(9–10), 2085–2113. https://doi.org/10.1016/s0967-0645(97)00092-1
- Van Den Broeck, N., Moutin, T., Rodier, M., & Le Bouteiller, A. (2004). Seasonal variations of phosphate availability in the SW Pacific Ocean near New Caledonia. *Marine Ecology Progress Series*, 268, 1–12. https://doi.org/10.3354/meps268001
- Van Wambeke, F., Christaki, U., Giannakourou, A., Moutin, T., & Souvemerzoglou, K. (2002). Longitudinal and vertical trends of bacterial limitation by phosphorus and carbon in the Mediterranean Sea. *Microbial Ecology*, 43(1), 119–133. https://doi.org/10.1007/s00248-001-0038-4
- Yoshimura, T., Ogawa, H., Imai, K., Aramaki, T., Nojiri, Y., Nishioka, J., & Tsuda, A. (2009). Dynamics and elemental stoichiometry of carbon, nitrogen, and phosphorus in particulate and dissolved organic pools during a phytoplankton bloom induced by in situ iron enrichment in the western subarctic Pacific (SEEDS-II). Deep Sea Research Part II: Topical Studies in Oceanography, 56(26), 2863–2874. https://doi.org/10.1016/j.dsr2.2009.06.011

HAGSTROM ET AL. 23 of 23